# X-ray Diffraction from Al Powder using Energy Dispersive Technique

by

Ibrahim S. Elyaseery, B.Sc.

A thesis
submitted to the Department of Physics
in partial fulfillment of the requirements
for the degree of
Master of Science

April 1991
Brock University
St. Catharines, Ontario

بسم الله الرحمن الرحيم

**To My Parents**

## Acknowledgements

I would like to thank Dr. J. Moore for giving me the opportunity to work with him and for his insight and help throughout. I would like also to thank the workers in the machine and the electronic shop for their help with the experimental apparatus.

## Abstract

Using the energy dispersive x-ray diffraction (EDXD) technique, the room temperature diffraction pattern of Al powder was obtained at diffraction angles ≈ 30° and 50°. From the small angle diffraction pattern the average relative intensities ($I_R$) of the (111), (200), and (220) lines were measured to be equal to 100, 62, and 32 respectively. From the large diffraction angle $I_R$ for the (220), (311+222), (400), (331+420), and (422) lines were measured to be 100, 201, 17, 90, and 19.5 respectively.

The diffraction pattern at those two angles were obtained at several higher temperatures to measure the change in the intensities of the Al lines. From the intensity changes the increase of the Debye- Waller temperature factor, i.e $\Delta B(T)$, with respect to the value at room temperature was determined to be 0.6±0.1 at 250°C, 1.10±0.15 at 350°C, 1.45±0.20 at 450°C, and 2.20±0.35 at 550°C.

# CONTENTS

## List Of Tables

## List of Figures

## (1) Introduction

The energy dispersive x-ray diffraction (EDXD) technique has developed greatly since it was first introduced by Giessen and Gordon in 1968[1]. They used a continuous x-ray beam from an x-ray tube to obtain the diffraction pattern of platinum (Pt) at a fixed angle. This technique was later used to measure precisely (.01%) the spacing between the planes (d) [2]. The technique is useful in detecting the effect of size of grains on the line broadening [3] and for detecting change of lattice constant as result of temperature change [4]. In more recent work by this technique, synchrotron radiation was used to produce a very intense beam. This was very valuable for the fast structure identification and studies of phase transformation at high temperature and high pressure [5,6,7]. Through the use of synchrotron radiation recognizable patterns could be obtained in a few seconds.

There has been a lot of experimental research done on Aluminum (Al) single crystal and powder to measure the relative intensities ($I_R$) and to investigate the Debye-Waller temperature factor (DWTF) [8,9,10]. The technique used in those experiments is angle dispersive x-ray diffraction [ADXD] in which a monochromatic x-ray beam is used. For the diffraction to occur in this technique, the crystal has to be rotated about its axis until it reaches a certain angle satisfying the diffraction condition for a certain plane. The EDXD technique differs in that aspect. In the EDXD a continuous x-ray beam is used. Therefore, diffraction occurs in a crystalline material held fixed at certain angle when different wavelengths satisfy the diffraction condition for different planes.

Because of this difference between the two techniques, there are advantages and disadvantages in using the EDXD rather than the ADXD [11,12]. The disadvantages are: It is more difficult to measure the relative intensity of different lines, since the intensities are measured at different regions of the energy spectrum where the incident beam intensity varies. Also, the resolution of the detector is poorer, as a result closely spaced lines cannot be resolved.

On the other hand, the advantages are : It is much faster to obtain a recognizable pattern of the material structure since all the diffraction lines appear simultaneously rather than waiting for the angular cycle to scan the crystal to obtain the complete diffraction pattern. The presence of a fluorescence line in the spectra would help in identifying the chemical nature of unknown material. Also, it is much easier to design an apparatus to carry out the diffraction measurement at high pressure and temperature, since no movement of the target or the detector is required.

X-ray diffraction is widely used as a tool for the study of the internal structure of materials. Through this method it can be determined whether the structure is crystalline or amorphous. Crystalline material means that the atoms are arranged in an ordered manner. The exact short range order arrangement of the atoms is repeated periodically through out the crystalline material. On the other hand, in amorphous material, there is short range order in the arrangement of the atoms however,there is no long range order [11,12,13].

X-ray diffraction is used most efficiently for the determination of the precise structure of crystalline materials. The structure is determined by the way the atoms are arranged in the unit cell of crystalline material. Also the diffraction technique could be used to measure the atomic displacements due to thermal vibration about their mean position within the unit cell. There are other parameters, holding information about the physical property of a substance, that can be determined by the x-ray diffraction technique. For example, x-ray diffraction can be used to determine the plane spacing (d) and the lattice constant (a) for the cubic structure. Through those two parameters, the type of the crystal lattice is identified whether it is simple cubic (sc), face centered cubic (fcc), or body centered cubic (bcc).

Diffraction phenomena result from the superposition of waves scattered by the atomic electrons without change taking place in their wavelength and leads to constructive interference in certain directions [11,12].

It was in 1912 that the first encounter with the phenomena of x-ray diffraction took place when Laue discovered that diffraction by a crystal occured if the wavelength of the x-rays were about equal to the separation distance of the atoms composing the crystal. Laue deduced three conditions for diffraction : $\mathbf{a}.\Delta\mathbf{K}=2\pi h$; $\mathbf{b}.\Delta\mathbf{K}=2\pi k$; $\mathbf{c}.\Delta\mathbf{K}=2\pi l$ [1,3,4], where($\mathbf{a},\mathbf{b},\mathbf{c},$) are the primitive lattice vectors, (h,k,l) are the Miller indices, and $\Delta\mathbf{K}$ is the change in the wave vector. Later Bragg verified Laue's theory, and he put the above three conditions in a very simple mathematical form : $2d \sin\theta = \lambda$.

The objective of this research is to establish, at Brock University, the energy dispersive x-ray diffraction (EDXD) technique as a tool for material analysis. To accomplish this objective, x-ray diffraction study of Al powder has been performed. Accurate and reproducible measurements of the relative intensities ($I_R$) of the diffraction lines are obtained at room temperature and compared to their corresponding theoretical values for the EDXD technique.

In the second part of the project measurements of the changes in the intensities of diffraction lines, resulting from temperature changes, have been performed and analyzed to determine the changes in the amplitude ($<u^2>$) of the thermal vibrations of the atoms about their mean position [11,12,13,14]. This is the Debye-Waller effect. The changes in the Debye-Waller temperature factor (DWTF) have been determined and then compared to the theoretical values.

The outline of this thesis is as follows: Chapter (2) presents the theory of diffraction and a description of the different factors which are involved in determining the diffraction intensity. Chapter (3) is a detailed description of the experimental apparatus employed in the experiment. Chapter (4) contains the different procedures carried out in the experimental work. Chapter (5) contains the experimental measurements of the intensities at room temperature and the analysis of the those measurements. In chapter (6) the experimental measurements of the temperature effect on the intensity and the analysis of those measurements is presented. Chapter (7) contains the conclusion.

## (2) Theory

The phenomenon of x-ray diffraction takes place when waves are scattered by the atomic electrons without change in their wavelength. A diffracted beam, which is the result of the superposition of those waves, is produced when a certain geometrical condition is satisfied. This condition is defined by the diffraction angle and the wavelength through Bragg's equation.

The resulting diffraction spectra are characteristic of the structure of the material. Information about the atomic structure of the crystal is extracted from the position and the intensity of the diffraction lines in the spectra. The positions of the lines determine the shape, the size, and the orientation of the unit cell. Measuring the intensity leads us to the position of the atoms within the unit cell [11]. Therefore, any displacement of the atoms about their mean position in the unit cell results in a change in the intensity of the diffracted beam.

### (2-1) Bragg Condition:-

For diffraction by a crystalline material to occur, the Bragg condition must be met. This condition states that there exist only certain angles ($2\theta$) at which an incident x-ray beam with wavelength $\lambda$ is diffracted. To understand how this condition is satisfied, let us consider a set of planes with (d) spacing. In those planes sit an array of atoms of spacing (a). X-rays of wavelength ($\lambda$) are incident on those planes at an angle ($\theta$) as shown in figure(2-1).

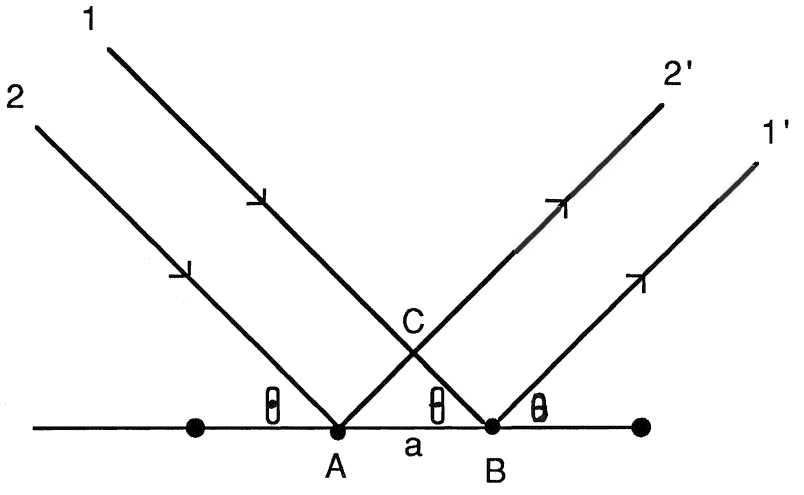


(a) The path difference between rays reflected by atoms in the same plane (AC-CB)=0

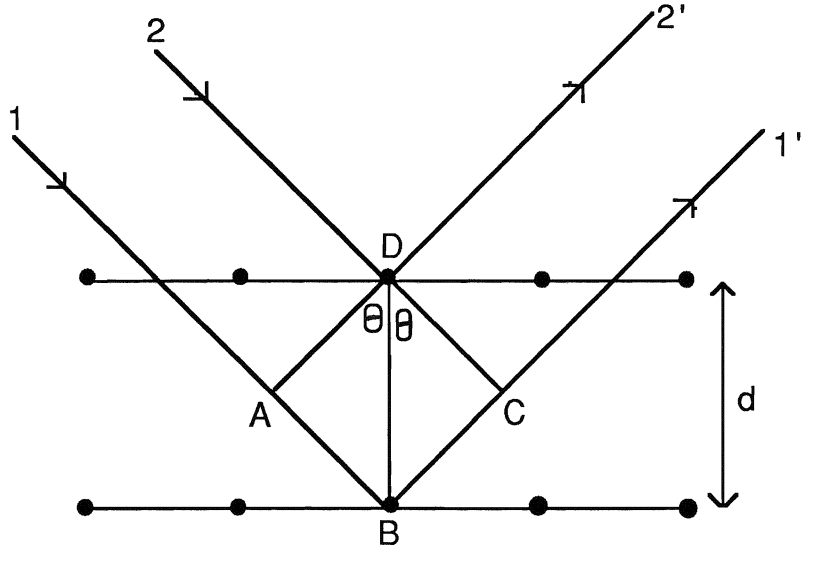


(b) The path difference between rays reflected by atoms in different planes (AB +BC) =2 d sinθ

Figure (2-1) The reflection of rays as required by the Bragg condition.

In figure (2-1a) rays 1 and 2 are incident on two atoms in the first plane. The path difference between those two rays at 1' and 2' is zero. Therefore, they are completely in phase. In figure (2-1b) rays 1 and 2 are scattered by atoms in different planes. The path difference between those two rays at 1' and 2' is given by

$$AB + BC = d \sin\theta + d \sin\theta = 2 d \sin\theta$$

The two rays at 1', 2' are completely in phase if their path difference is equal to an integer number (n) times the wavelength of the incident rays i.e

$$2 d \sin\theta = n \lambda$$

This is the Bragg condition for constructive interference resulting in diffraction. If any order of reflection is considered as first order( n=1) from a plane at a distance d from the previous plane, then the Bragg condition is written as

$$2 d \sin\theta = \lambda$$

The Bragg Equation For The EDXD:-

For the ADXD technique the wavelength($\lambda$) is constant, and the diffraction angle ($\theta$) is variable in the above Bragg equation. So, for planes of different (d) spacings the diffraction occurs at different angles. In the case of the EDXD technique the incident x-ray beam is not monochromatic, i.e it contains x-ray photons of different wavelengths. Therefore, the Bragg condition could be satisfied at a fixed diffraction

angle for planes of different (d) spacing [11,12]. With the energy of the x-ray photon given as E= (hc/λ),the Bragg equation is written as

$$E.d = (hc/2\sin\theta) = \text{constant}.$$

## (2-2) Intensity Of The Diffracted Beam:-

When diffraction occurs, the wavelength of the diffracted beam remains the same as that of the incident beam. However, the intensity of the diffracted beam will be different from that of the incident beam. The intensity of the diffracted beam is determined by several factors. These factors are:

1-The structure factor. (F)

2-The atomic scattering factor. (f)

3-The absorption factor. (A)

4-The multiplicity factor. (P)

5-The polarization and Lorentz factors.

6-The temperature factor. (exp[-2M])

### (1) The structure Factor (F) :-

A crystal is invariant under translation vector $\mathbf{T}=u\mathbf{a}+v\mathbf{b}+w\mathbf{c}$ where u, v, w are integers. The electron number density $n(\mathbf{r})$ is a periodic function of position $\mathbf{r}$ with periods a, b, c in the direction of the crystal axes. $n(\mathbf{r})$ experessed in a fourier series is [13]

$$n(\mathbf{r}) = \sum_{G} n_G \exp[i\ \mathbf{G}.\mathbf{r})]$$

$\mathbf{G} = h\mathbf{A} + k\mathbf{B} + l\mathbf{C}$ is a reciprocal lattice vector, where **A**, **B**, **C** are the primitive vectors for the reciprocal lattice.

$n(\mathbf{r})$ is invariant under **T** i.e

$$n(\mathbf{r}+\mathbf{T}) = \sum_{G} n_G \exp[i\ \mathbf{G}.\mathbf{r})] \exp[i\ \mathbf{G}.\mathbf{T}], \quad e^{i\mathbf{G}.\mathbf{T}}=1$$

$$= \sum_{G} n_G \exp[i\ \mathbf{G}.\mathbf{r})] = n(\mathbf{r})$$

A crystal by definition is a repetition of the fundamental unit cell [11,13]. Therefore, the effect of the atomic arrangement in the unit cell on the intensity of the diffracted beam is considered. The reciprocal lattice vectors **G** determine the possible x-ray reflections, through the diffraction condition. $\Delta\mathbf{K} = \mathbf{G}$. The amplitude of scattering from a unit cells defined as the structure factor F [13]

$$F = \int dv\ n(\mathbf{r}) \exp[-i\ \mathbf{G}.\mathbf{r}]$$

For a unit cell containing N atoms the contribution to the electrons concentration from those atoms at a position **r** is given as

$$n(\mathbf{r}) = \sum_{j}^{N} n_j(\mathbf{r}-\mathbf{r}_j), \quad \text{substituting in F}$$

$$F = \sum_{j} \exp[-i\ \mathbf{G}.\mathbf{r}_j] \int dv\ n_j(\mathbf{r}') \exp[-i\ \mathbf{G}.\mathbf{r}']$$

where $\mathbf{r}' = \mathbf{r}-\mathbf{r}_j$

The atomic scattering factor $f_j$ is $\int dv\ n_j(\mathbf{r}')\ \exp[-i\ \mathbf{G}.\mathbf{r}']$

Therefore,

$$F = \sum_j f_j \exp[-i\ \mathbf{G}.\mathbf{r}_j)]$$

Substituting for $\mathbf{G}$ and $\mathbf{r}_j$

$$F = \sum_{j=1}^{N} f_j \exp[-2\pi i(hx_j+ky_j+lz_j)].$$

F is the structure factor which holds the information about the unit cell regarding the position arrangement of the atoms. The intensity of the diffracted beam is proportional to the square of the absolute value of (F), i.e $I \alpha |F|^2$.

(2) The Atomic Scattering Factor (f) :-

Diffraction is the result of elastically scattered reinforced waves. This takes place when the incident x-rays causes the electrons to oscillate about their mean position [11]. The oscillatory motion of the electrons cause them to emit electromagnetic radiation. The wavelength of the emitted electromagnetic radiation is the same as that of the incident rays. Therefore, the scattered x-rays making up the diffracted beam are emitted by the electrons which encounter the incident x-ray beam.

The incident beam interacts with electrons located at different positions in the atom. Therefore, the wave scattered by the atom is the interference sum of the waves scattered by different electrons in the atom. Figure (2-2) shows the scattering by two electrons at different positions in

the atom. If the scattering occurs in the forward direction (i.e 2θ=0), then the path difference is zero resulting in the scattered waves being in phase. Scattering in other directions causes a difference in the path of the scattered waves which results in the waves being out of phase.

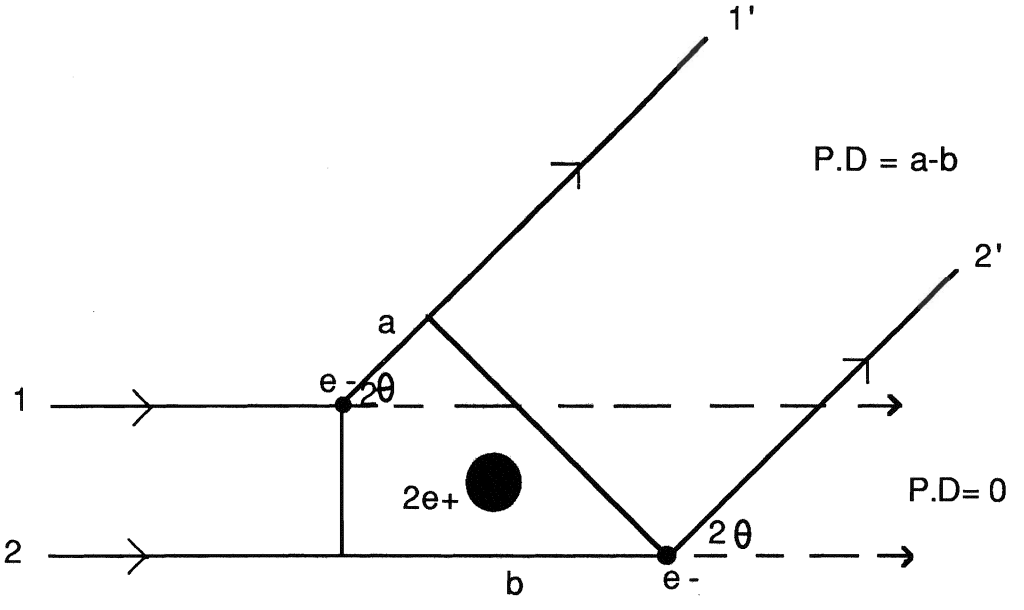


Figure (2-2) The scattering of waves by electrons at different position in the atom.

The efficiency of scattering by the electron distribution of an atom for a particular direction is given by the atomic scattering factor (f). f is a function of the spatial distribution of the atomic electrons n(r) and gives the ratio of the amplitude of scattered wave by an atom to the amplitude of the scattered wave by an electron [11,13].

$$f = 4\pi \int n(r)\, r^2 \frac{\sin Gr}{Gr}\, dr$$

The two factors which affect the value of f are the diffraction angle ($2\theta$) and the wavelength ($\lambda$). An increase in the diffraction angle results in the scattered waves becoming more out of phase, hence the value of f decreases. At a fixed $\theta$, the value of f decreases as $\lambda$ decreases. The combined effect of $\theta$ and $\lambda$ on f is given as ($\sin\theta/\lambda$). In the case of scattering in the forward direction (The reciprocal lattice vector G=0), f is a maximum and equal to the number of the electrons in the atom. Figure (2-3) shows the relation f vs. ($\sin\theta/\lambda$) for Al.

(3) The Absorption Factor (A):-

The intensity of the diffracted beam is affected by the absorption process the beam undergoes within the sample. This absorption factor is usually written as function of ($\theta$) for some diffraction techniques. On the other hand, this factor is independent of ($\theta$) in the diffractometery technique since the volume of the sample exposed to the beam stays constant even if ($\theta$) is changed [11,12,15].

To calculate the absorption factor, let us consider the absorption process taking place in the sample shown in figure (2-4). An x-ray with intensity $I_0$ is incident on the sample. It is diffracted by a portion dx at a distance x inside the sample. The incident ray undergoes absorption to reach dx. Now, the diffracted ray from dx is given as

$$dI' = C\, I_0 \exp[-\mu S]\, \frac{dx}{\sin\theta}.$$

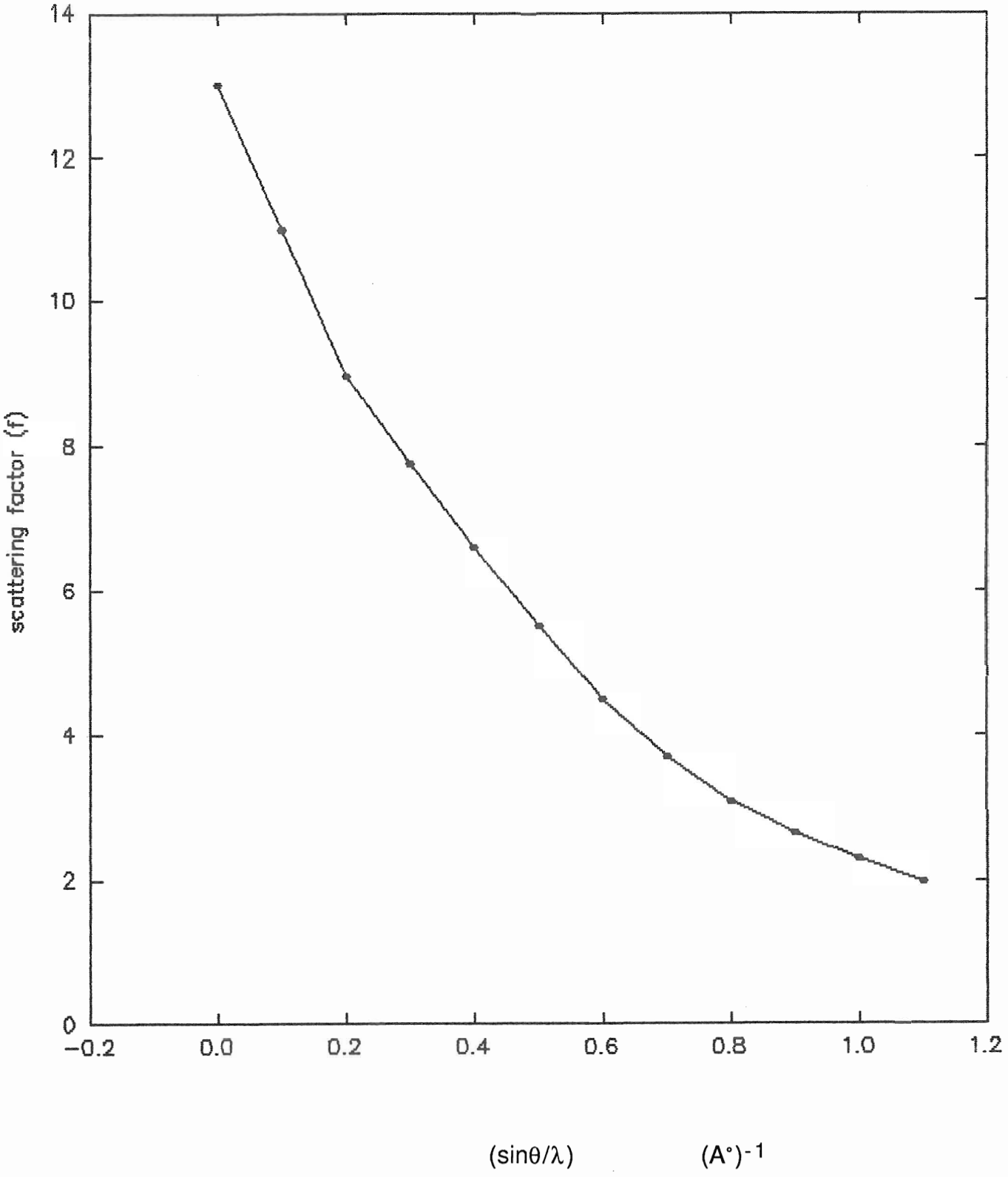


Figure(2-3) The relation between scattering factor (f) and ($\sin\theta/\lambda$) for Al.

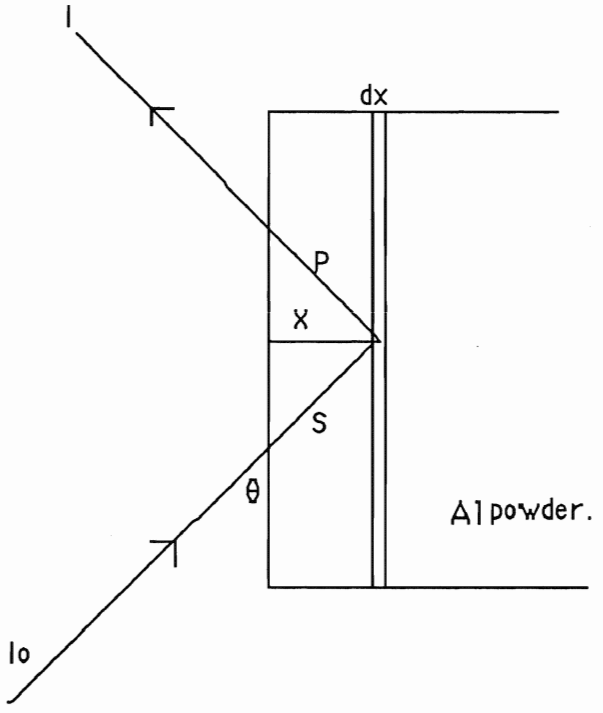


Figure (2-4) The absorption process in the sample.

The intensity of this ray leaving the sample is

$$dI = dI' \exp [-\mu P]$$

$\mu$ is the linear absorption coefficient.

$S = x/\sin\theta$ is the distance travelled by the incident ray in the sample.

$P = x/\sin\theta$ is the distance travelled by the diffracted ray in the sample.

C is the constant of diffraction.

The intensity of the ray diffracted by the sample is

$$I = \frac{CI_0}{\sin\theta} \int_0^{\infty} \exp[-2\mu x/\sin\theta]dx.$$

$$I = \frac{CI_0}{2\mu} \quad \text{i.e} \quad I \alpha 1/\mu.$$

In calculating the $I_R$ using a monochromatic beam, the effect of the absorption factor is the same for all the diffraction lines. Therefore,this factor's effect on the $I_R$ cancels out. On the other hand , in EDXD which uses a continuous x-ray beam, the absorption factor enters into the calculation of $I_R$. Figure(2-5) shows the mass attenuation coefficient($\mu/\rho$) for x-ray photons of various energies in Al [16].

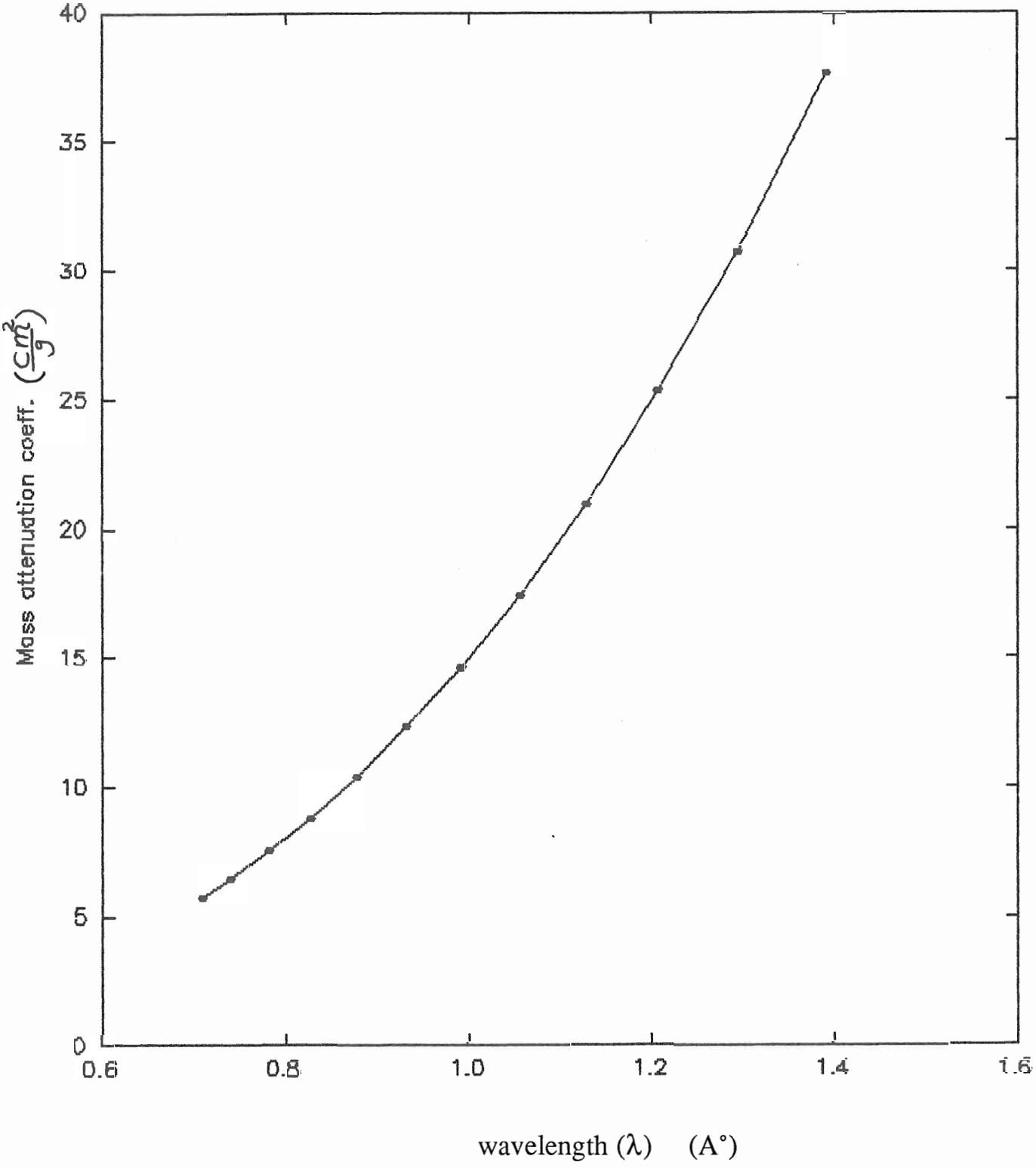


Figure (2-5) The absorption of Photons of different wavelengths in Al

(4) The Multiplicity Factor (P):-

This factor which influences the intensity of the diffraction is defined as the number of different planes having the same plane spacing $d_{(hkl)}$ [11,12]. The Bragg condition could be satisfied by several planes which have the same (d) value but have different (hkl) values. Those planes will contribute to the intensity of the same diffraction line. Al, which is a cubic lattice, contains different planes with identical $d_{(hkl)}$. For example, the planes (100), (010), and (001) are separated by the same distance, even though they are denoted by different Miller indices.

The value of P depend also on the type of crystal system or symmetry as shown in table (2-1) which contain the P factor for various types of crystals [11].

**Table (2-1):-**

The multiplicity factor for different types of crystals.

| Crystal | Planes | | | | | | |
|---|---|---|---|---|---|---|---|
| Cubic | hkl | hhl | 0kl | 0kk | hhh | 00l | |
| P | 48 | 24 | 24 | 12 | 8 | 6 | |
| Hex.Rh. | hk.l | hh.l | 0k.l | hk.0 | hh.0 | ok.0 | 00.l |
| P | 24 | 12 | 12 | 12 | 6 | 6 | 2 |
| Tetra. | hkl | hhl | 0kl | hk0 | hh0 | 0k0 | 00l |
| P | 16 | 8 | 8 | 8 | 4 | 4 | 2 |

Note:- (hhl)=(hkl) where h=k and it is equivalent to (hkk).

(5) The Lorentz And Polarization Factors:-

These two factors affect the intensity of the diffracted beam as a result of geometrical changes in the orientation of the beam and the target.

The polarization factor arises whenever the incident beam is unpolarized. X-rays produced by x-ray tubes are unpolarized. Therefore, the polarization factor has to be introduced into the calculation of the intensity of the diffracted beam. This factor is introduced to correct for the change that occurs in the orientation of the electrical field vector components in the diffracted beam. This correction is introduced as [11,12]

$$\frac{(1 + [\cos 2\theta]^2)}{2}$$

The Lorentz factor (L.F) is a geometrical factor which is made up of three contributions [11]. One arises from the rotation of the crystal through the Bragg angle range ($\Delta\theta$). The product of the $I_{max.}$ and the width at half maximum of the line (B), which give the integrated intensity of diffraction line, depend on this angle range. With $I_{max.} \alpha (1/\sin\theta)$ and $B \alpha (1/\cos\theta)$. The product is $(1/\sin 2\theta)$. The second contribution is related the number of crystals ($\Delta N$) which have the correct orientation in the angle range ($\Delta\theta$) to contribute to the reflection out of total number (N) with $\Delta N/N$ is given as $(\Delta\theta.\cos\theta)/2$. Hence, $\Delta N \alpha \cos\theta$. The third contribution deals with the relative intensities in which the integrated intensity per unit length is proportional to $(1/\sin 2\theta)$. Therefore, from those quantities the lorentz factor is

$$L.F = (1/\sin 2\theta).(\cos\theta).(1/\sin 2\theta) = \frac{1}{4.\sin^2\theta.\cos\theta}.$$

(6)The Temperature Factor (exp[-2M]):-

In reality there is no crystal where the atoms sit motionless in their planes. Atoms undergo thermal vibration about their equilibrium position even at room temperature. The atomic displacements or vibrations about the mean position affect the diffraction intensity.

Increasing the temperature leads to the increase of the mean square displacement $\langle u^2 \rangle$ of the atoms resulting in irregularities in the atomic planes. Consequently, the intensity of the diffracted beam is reduced.

The temperature effect is introduced into the calculation of the diffraction intensity via an exponential factor (exp[-2M]). To calculate this factor, let us consider a lattice point with position ($\mathbf{r}_i$) from the origin. This point is displaced from its equilibrium position with displacement ($\mathbf{u}_i$). The new position is given as ($\mathbf{r}_i+\mathbf{u}_i$) from the origin. The contribution to the structure factor from this point is [13,14]

$f \exp[-i\mathbf{G}.\mathbf{r}_i] \exp[-i\mathbf{G}.\mathbf{u}_i]$ ___(1), where $\mathbf{G}$ is the reciprocal lattice vector.

In taking the average, only the second exponential is averaged since the first is constant with time. Letting $\mathbf{G}.\mathbf{u}_i = p$, the mean of the exponential could be expanded as

$$\langle \exp[-iP] \rangle = 1 - \langle iP \rangle - \frac{\langle P^2 \rangle}{2} + \ldots\ldots\ldots$$

$\langle P \rangle = 0$, for odd power since the displacement is random, then

$$\langle \exp[-iP] \rangle = 1 - \frac{\langle P^2 \rangle}{2} + \frac{\langle P^4 \rangle}{24} + \ldots\ldots$$

$$\approx \exp[-\frac{\langle P^2 \rangle}{2}], \quad \text{where}$$

$$\langle P^2 \rangle = \langle (\mathbf{G}.\mathbf{u}_i)^2 \rangle = G^2 \langle u_i^2 \rangle \langle (\cos\theta)^2 \rangle$$

$$\langle (\cos\theta)^2 \rangle = \frac{1}{3}, \quad \text{for averaging over all directions.}$$

Eq. (1) is now $f \exp[-i\mathbf{G}.\mathbf{r}_i] \exp[-\frac{1}{6} G^2.\langle u_i^2 \rangle]$

The intensity of the diffraction is $I \alpha |F|^2$

$$I \alpha f_i^2 \exp[-\frac{1}{3} G^2.\langle u_i^2 \rangle],$$

$$\frac{1}{3} G^2.\langle u_i^2 \rangle = \frac{1}{3} (2\pi/d)^2.\langle u_i^2 \rangle$$

$$= \frac{16}{3} \pi^2 (\sin\theta/\lambda)^2 \langle u_i^2 \rangle = 2M$$

$$M = \frac{8}{3} \pi^2 \langle u_i^2 \rangle (\sin\theta/\lambda)^2$$

$$B(T) = \frac{8}{3} \pi^2 \langle u_i^2 \rangle$$

$M = B(T).(\sin\theta/\lambda)^2$, where B(T) is the DWTF.

Now, $I \alpha f_i^2 \exp[-2M]$.

In table (2-2) are the calculated values of B(T) for Al worked out by Shukla and Hubschle [17]. Those values of B(T) are used for the calculation of the intensity which will be compared to the experimental intensity.

**Table (2-2):-**

The values of B(T)for Al, obtained by the Green's function method, are shown as function of temperature (T) for different two bodies potentials.

| T (K) | AVS. $(A°)^2$ | AH. $(A°)^2$ | HHS. $(A°)^2$ | Morse $(A°)^2$ |
|---|---|---|---|---|
| 300 | 0.9554 | 0.9573 | 0.9875 | 0.8434 |
| 450 | 1.5004 | 1.5074 | 1.5816 | 1.3088 |
| 600 | 2.0703 | 2.0860 | 2.2199 | 1.8114 |
| 750 | 2.6399 | 2.6668 | 2.8864 | 2.3595 |
| 850 | 3.0022 | 3.0422 | 3.3285 | 2.7558 |

The values of B(T) in the above table were obtained from the calculation of $\langle u^2 \rangle$ by using an Ashcroft pseudopotential with Habbard (AH) and Vashishta-Singwi (AVS) electron-gas screening functions $\varepsilon(q)$, a Harrison modified point ion pseudopotential with Habbard-Sham (HHS) screening function, and a nearest neighbour central force three parameter Morse potential [17]. In comparing the calculated values of B(T) from these different potentials with experimental values which were obtained by different methods, the values of B(T) corresponding to the HHS potential show the closest agreement. On the other hand, the values of B(T) corresponding to Morse potential show the least agreement [17]

## (2-3) Intensity Expression for EDXD:-

The intensity equation for the diffracted beam from a crystalline material, taking into account all the factors mentioned previously, is given as [11]

$$I_{total} = I_0 \left[\frac{A\lambda^3}{32\pi r}\left(\frac{\mu_0}{4\pi}\right)^2 \frac{e^4}{m^2}\frac{1}{v^2}\right] |F|^2 P \left[\frac{(1+[\cos 2\theta]^2)}{\sin^2\theta.\cos\theta}\right] e^{-2M}.\frac{1}{2\mu} \quad \text{------(*)}$$

v is the volume of unit cell, m is mass of electron, e charge of electron, A is the cross-sectional area of the incident beam, and r is the radius of the diffractometer circle.

In the expression of $I_R$ of different diffraction lines for the ADXD technique, the incident beam intensity ($I_0$) and the linear absorption coefficient ($\mu$) are constant. Therefore, they are omitted from the $I_R$ expression which is given as [11,12]

$$I_R = |F|^2 P \left[\frac{(1+[\cos 2\theta]^2)}{\sin^2\theta.\cos\theta}\right] \exp[-2M].$$

The Modified Expression Of $I_R$ For The EDXD:-

In this particular technique, a continuous x-ray beam is used and the diffraction angle is held constant. The Bragg condition is satisfied for different planes at different energies in the spectrum of the incident beam. Consequently, to calculate the $I_R$, the fact that the incident intensity $I_{o(hkl)}$ and the linear absorption coefficient $\mu_{(hkl)}$ will vary from one line to another must be taken into account. On the other hand, since the diffraction angle is fixed, the Lorentz-polarization factor is constant and therefore is omitted from the $I_R$ expression.

Another change in the $I_R$ expression is due to the natural width of the line ($\Delta E$) which is defined by the system acceptance angle ($\Delta\theta$) as shown in figure(2-6). In EDXD, the Bragg equation is

$$E = \frac{h.c}{2d\ \sin\theta}.$$

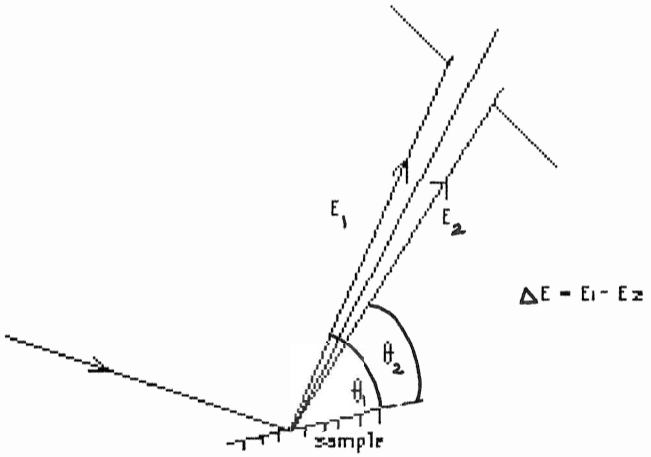


Figure (2-6) The slit acceptance angle defining the width of the peak

The diffraction maximum is met at E; however, as a consequence of the finite acceptance angle the diffraction condition is still satisfied at small energy interval below and above E. The change in energy with respect to the diffraction angle is

$$(dE/d\theta) = \frac{hc}{2d}\left(\frac{-\cos\theta}{\sin^2\theta}\right)$$

$$= - \frac{E}{\tan\theta}.$$

The energy interval corresponding to $\Delta\theta$ is therefore

$\Delta E = E \left(\frac{-\Delta\theta}{\tan\theta}\right)$ ; the diffraction angle is fixed for all diffraction lines, and so

$$\Delta E = (\text{constant})\ E.$$

Since the EDXD technique uses a continuous beam, then

$$I \ \alpha \ \Delta E.$$

Also $I \ \alpha \ \lambda^3$, so

$$I_R \ \alpha \ \lambda^3 . \Delta E$$

$$I_R \ \alpha \ 1/E^3 . E \ \alpha \ 1/E^2$$

Hence, the complete expression of $I_R$ is

$$I_R = (I_0 \varepsilon) |F|^2 P \exp[-2M] (1/\mu) (1/E^2).$$

## (3) Experimental Apparatus

The apparatus system employed for the x-ray diffraction study basically consists of an x-ray tube, a target assembly, and an x-ray spectrometer system. Figure (3-1) shows a schematic diagram of the apparatus system.

### (3-1) X-Ray Tube :-

A (Mo) target tube, with maximum operational voltage of 60 kV and power of 2400 w, is used in this assembly as source of the x-ray beam. The x-ray beam is produced when electrons are accelerated to high kinetic energy through the potential difference between the cathode and the anode. Those energetic electrons will undergo collision with the anode's atoms. The kinetic energy of the electron on impact is given as

$$K.E = eV, \text{ where V is the potential difference.}$$

The electrons lose their energy in collisions with the anode's atoms by a bremsstrahlung process. In this process some electrons are stopped in one collision thereby losing all their energy. Other electrons lose a fraction of their energies successively through different collisions. The deceleration of the electrons results in x-ray photons having wavelength ($\lambda$) corresponding to the energy lost $.E = (hc)/\lambda$ [12]. The spectrum of the x-ray beam produced by the bremsstrahlung process will consist of continuous energy distribution. Figure (3-2) shows the product of the energy spectrum of the incident beam produced by the Mo tube at 20 kV and the detector efficiency ($\varepsilon$).

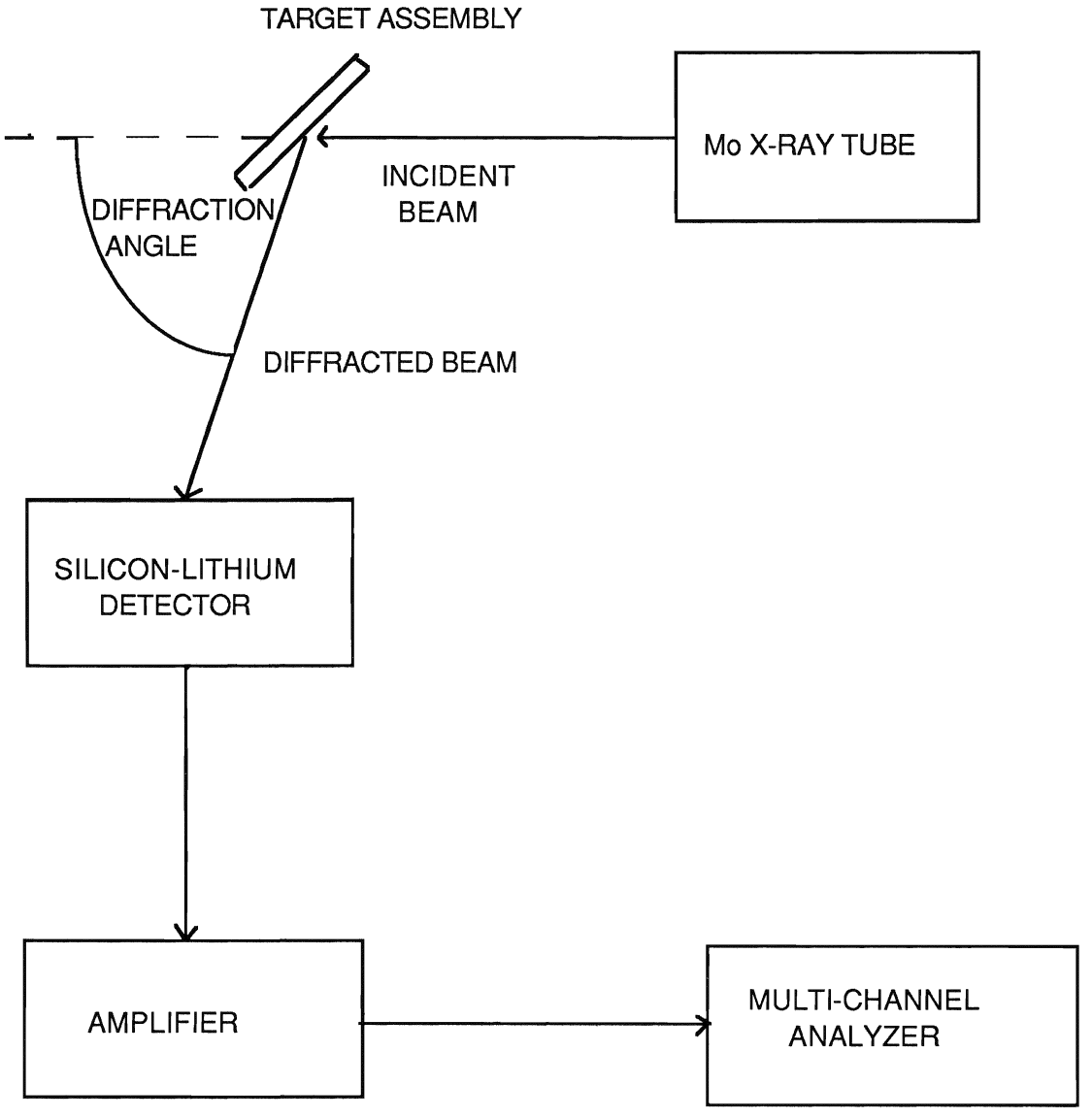


Figure (3-1) A schematic diagram of the apparatus system

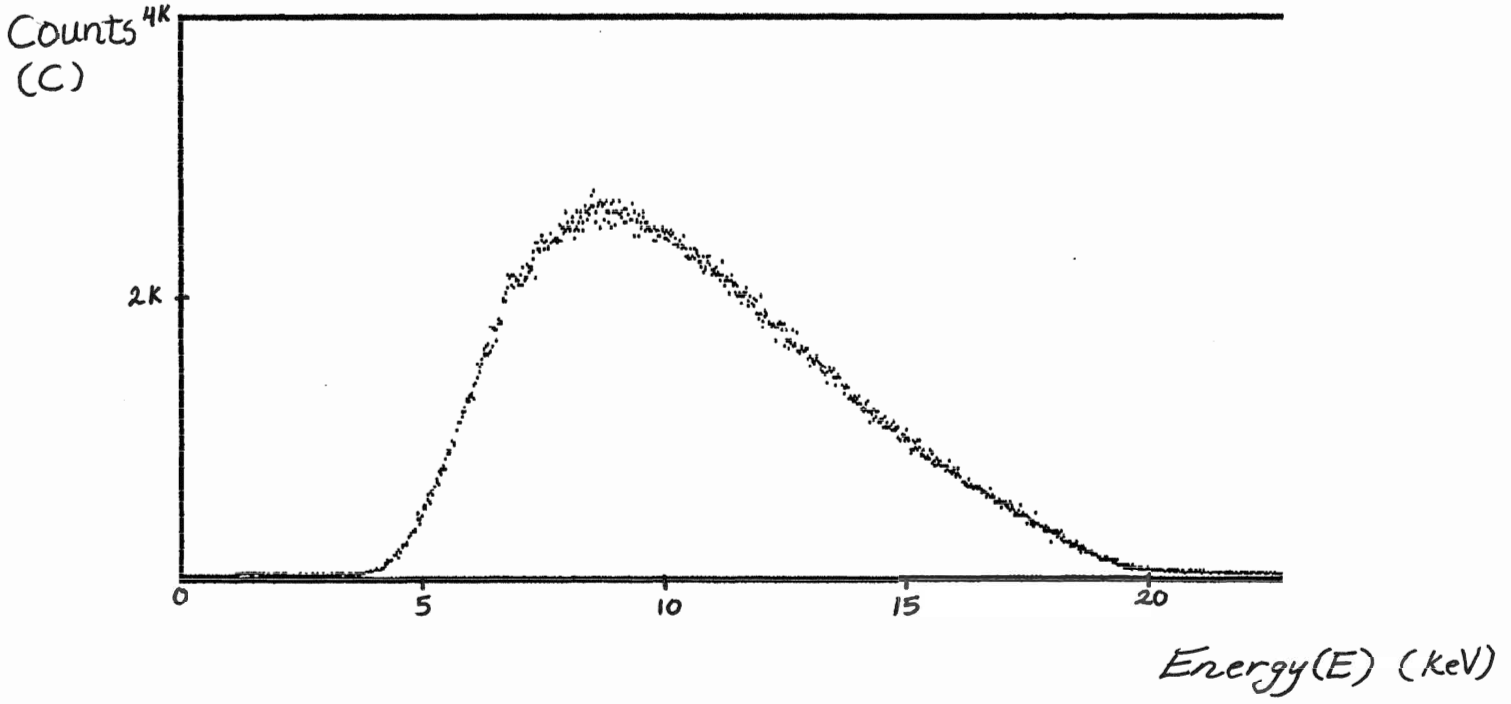


Figure (3-2) The energy spectrum of the product of the incident beam intensity and the detector efficiency. The spectrum is E (< 20 keV) vs. counts (4 k).

When the kinetic energy of the electrons is higher than the binding energy of the inner shell electrons (for example the binding energy of the k-shell electrons in Mo is 20 keV), the tightly bound electrons are knocked out thereby exciting the atom. A transition process takes place by the electrons from the outer shells to the produced vacancies resulting in the emission of x-ray photons characteristic of the Mo atom. When this process takes place for the Mo tube, the spectrum of the x-ray beam will consist of sharp characteristic lines sitting on top of the high energy region of the continuous spectrum curve shown in figure (3-2). The lines are $K_\alpha$ and $K_\beta$ of Mo having energies of 17.441 and 19.605 keV respectively.

The x-rays produced are emitted in all directions. A fraction of those rays pass through a 14.5 mm window and then through a very narrow (1mm) collimator in order to produce an intense beam with well defined direction.

## (3-2)Tungsten (W) Contamination Of The Mo Tube :-

In order to carry out diffraction analysis using the EDXD technique, the spectrum of the incident x-ray beam has to be clean and smooth, and it must not be contaminated with characteristic lines. When the first diffraction measurements were carried out, the data obtained showed the presence of several characteristic lines in the spectra. Those lines were identified to be $L_\alpha$ and $L_\beta$ of W. The source of those lines was identified to be the Mo tube itself. It was concluded that as result of the long use of the Mo tube, a contamination of the anode by W from the cathode occured.

The only way to eradicate this problem is by obtaining a new tube for the diffraction analysis. Therefore, a new Mo tube was installed in the EDXD apparatus system. Figure (3-2) was obtained from the new tube in which the W contamination was eliminated.

## (3-3) Target assembly:-

There are two target assemblies for two different functions.

### (1) Room Temperature Assembly:-

This assembly is for the purpose of the experimental measurements done at room temperature. Therefore, this assembly is for carrying out the first part of the research to measure the relative intensities of the Al powder diffraction lines.

It basically consists of a brass holder for the Al powder and a mount for the holder. The brass holder is made up of two pieces. Figure (3-3) shows the two pieces of the sample holder. The first piece is a thin disc (3 mm thickness) with a hole (20 mm diameter ) in the middle. The purpose of this hole is for carrying the Al powder. The second piece is a solid disc of the same size as the first piece. This solid disc is connected to the first piece in order to keep the powder from falling apart or spilling. The purpose of choosing 3 mm thickness of the disc is to allow enough powder thickness so that no significant transmission of the incident beam takes place thereby eliminating diffraction effect from the holder itself. This sample holder is mounted on a 10 R.P.M motor for the purpose of rotating the sample. The motor is connected to the mount assembly as

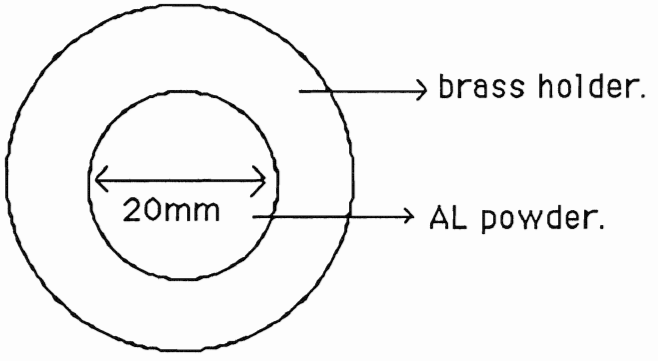


(a) Top view of the sample holder.

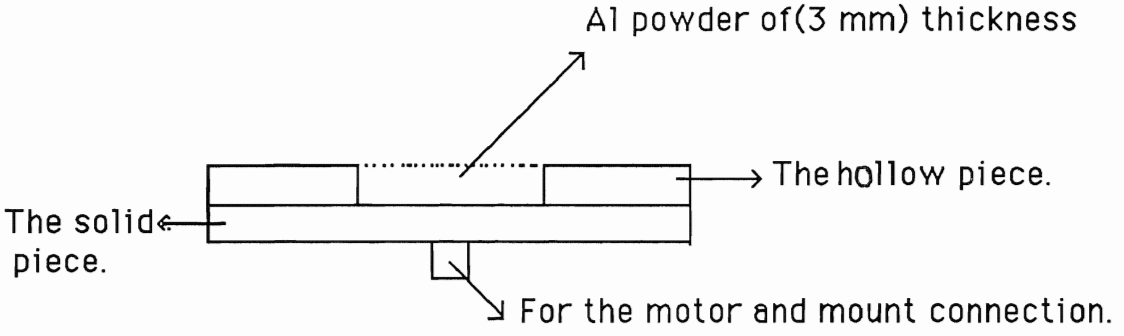


(b) Side view of the sample holder made up of the two pieces.

Figure (3-3) the sample holder.

shown in figure (3-4). This mount assembly allows for the manual adjustment of the sample in the degrees of freedom needed

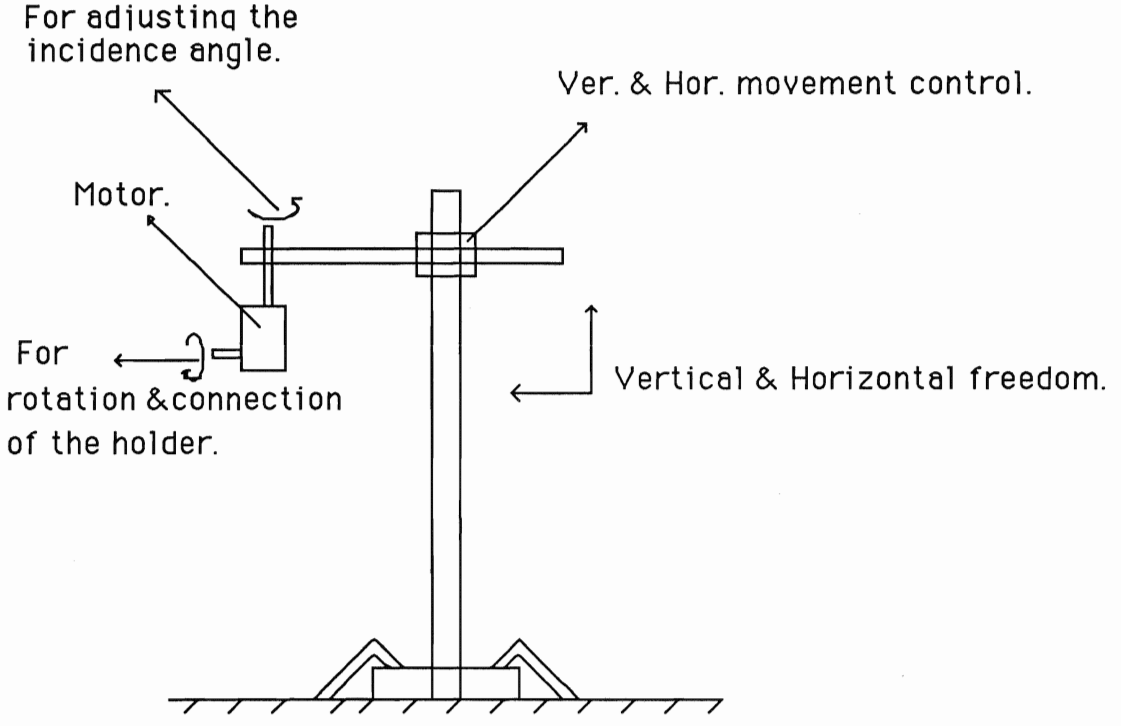


Figure (3-4) a schematic diagram of the target mount.

(2) High Temperature Assembly:-

In order to carry out x-ray diffraction measurements at high temperature, a system for heating and controlling the temperature of the sample is needed. The device for heating the Al powder has to be operated in conditions that minimize the oxidation of the Al powder. Therefore, the heating process has to be carried out under vacuum.

The operation of the system under vacuum raises a problem. This problem is the exposure of the heated target to the incident beam and the detection of the diffracted beam by the detector. Hence, entrance and exit windows have to be part of the heating and the vacuum system. The material of the window must have low absorption, must resist low pressure, and have the ability to function at high temperature. This system which is shown in figure (3-5) is made up of:

(1) A brass vacuum cell which has a diameter of 150 mm and a height of 220 mm. The cell has three small (5 mm) entrance windows and one larger exit window (10 mm). The combination of each one of the entrance windows and the exit window allows for the freedom to chose different diffraction angles ($2\theta$). The combinations allowed are: $30^{\circ}$, $50^{\circ}$, $70^{\circ}$. The material of the window is very thin ( o.1 mm ) mylar sheet which is known for its low absorption of x-rays.

(2) The heating and target holder system which is made up of a small heater block made of copper (Cu). The Cu block is heated by three firerod cartridge heaters which are immersed into it. The size of those heaters is 6.25 mm in diameter and 38.1 mm in length. Each supplies a

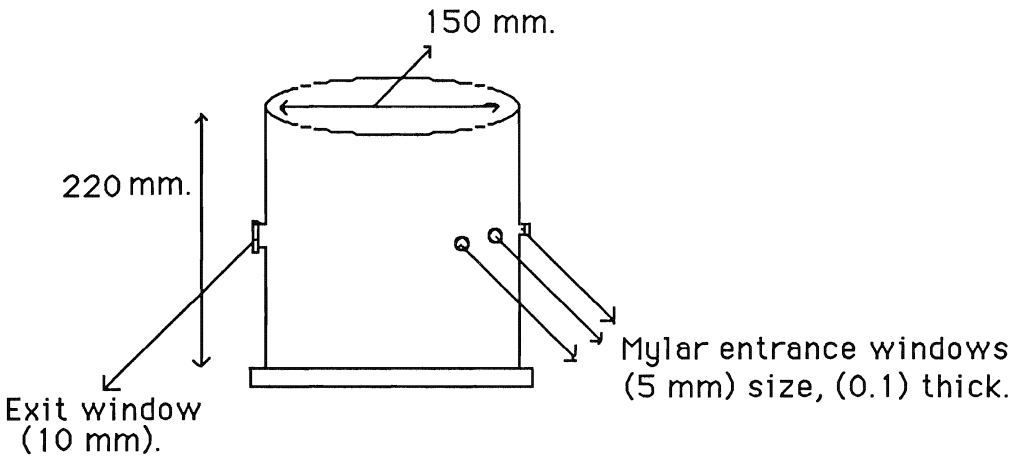


(a) The brass vacuum cell.

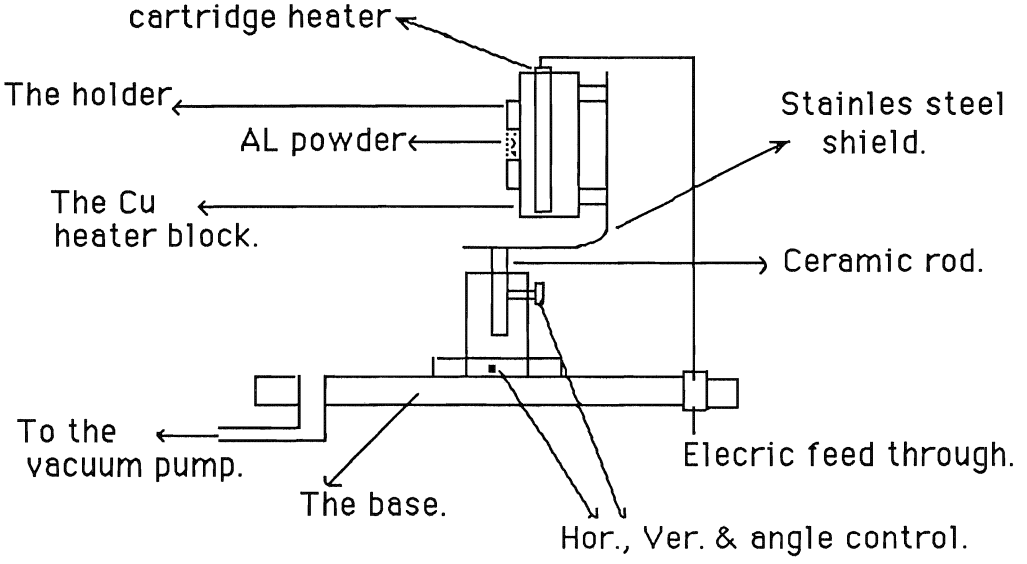


(b) The base & heating system.

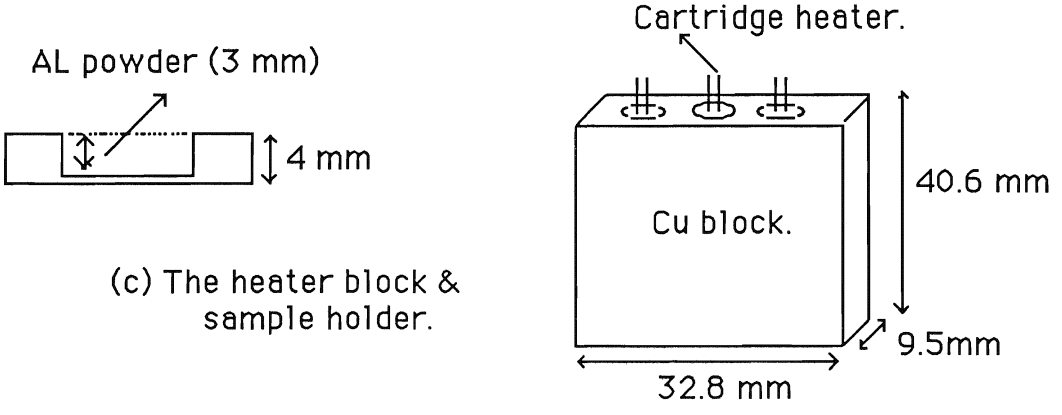


(c) The heater block &
sample holder.

Figure (3-5) The temperature apparatus

power of 200 w which is more than enough to heat the Cu block and the Al powder up to the maximum temperature needed. On this heater block, the Al powder holder is mounted. The holder is a hollow disc (4 mm ) made of Cu. The disc holds the Al powder of 3 mm thickness and 20 mm diameter. The heater block and the powder holder are mounted on a stainless steel shield which is fixed to the base by a ceramic rod to insulate the heater block from the rest of the apparatus. This assembly permits the movement of the target in all the degrees of freedom necessary to carry out the experimental measurements.

(3) The power supply and temperature monitoring system which consist of a (thermo-electric 400) temperature control device . This device is connected to the cartridge heaters for the purpose of supplying the electric power, and it is also connected to the sample holder by a chromel-alumel thermocouple for the purpose of measuring and controlling the temperature. An independent measurement of the temperature of the sample is made by another Chromel-alumel thermocouple connected to a Hewlett-Packard [3465A] digital multimeter.

(4)The base, which carries the heater block and the target, has two openings. One is for the electric feed through to the power supply and the temperature monitor. This opening is vacuum sealed with epoxy cement. The second opening is for the vacuum pump. The base is fixed upon the axis of rotation of the detector to permit the change in the diffraction angle. The brass vacuum cell is positioned on this base to seal the whole system.

(5) The vacuum system consists of an oil vacuum pump and thermocouple gauges. The lowest pressure obtained by the oil pump is approximately 10-15 μ of Mercury.

## (3-4) The X-Ray Spectrometer System:

It consists of the detector and multi-channel analyzer system.

(1) The Detector :-

To detect the x-ray photons with energies corresponding to the diffraction lines, an EG+G ORTEC Si(Li) detector is used [18]. This detector consists of a 5 mm thick lithium-drifted silicon Si(Li) crystal, pre-amplifier, 0.025 mm thick beryllium (Be) window which has a diameter of 10 mm, and liquid nitrogen dewar. The detector is operated at liquid nitrogen temperature (77 K) and a voltage of 1000 v.

(a) Detector Operation:-

The detection of the x-ray photons occurs when the impinging photons create electron-hole pairs in the Si(Li) detector [12]. The number of these generated pairs is proportional to the energy of the absorbed photon. The electron-hole pairs are separated then attracted to the detector electrode of opposite charge, thus producing a voltage pulse. The amplitude of the pulse is in turn proportional to the number of the electron-hole pairs, hence it is also proportional to the energy of the absorbed photon. The pulses produced are then treated and amplified by the pre-amplifier.

(b) Detector Resolution:-

The energy resolution of the detector is very important feature as far as the diffraction measurement is concerned. Depending on the performance of the energy resolution of the detector, it could be determined whether or not closely spaced diffraction lines are resolved. The energy resolution of this particular detector is given by the manufacturer as 180 eV [18]. This detector resolution cannot resolve very closely spaced diffraction lines in the Al pattern.

The performance of the detector resolution is monitored regularly. This is done by measuring the width at half -maximum of the $K_\alpha$ peak of Mn which is obtained from the energy spectra of $Fe^{55}$ source. The measured energy resolution was found to be in the range of 170-180 eV.Therefore, the resolution performance is very good. Figure (3-6) hows how the resolution of the detector is measured in the Fe source spectra.

( c) Detector Efficiency:-

There are two factors which determine the efficiency of the detection of the x-ray photons of various energies. The efficiency is influenced by the thickness of the Si(Li) detector and the Be entrance window. Figure (3-7) shows the graph of the efficiency of the detection of photons of different energies by the Si(Li) detector and Be windows of various thickness [18]. For our particular detector, the efficiency is 100% in the energy range of 5-20 keV. This is the region where the diffraction lines of Al will concentrate. Below this region the efficiency is affected by the absorption of the photons by the Be window and above it the efficiency drops as result of the decrease in the photon absorption in the Si depletion layer.

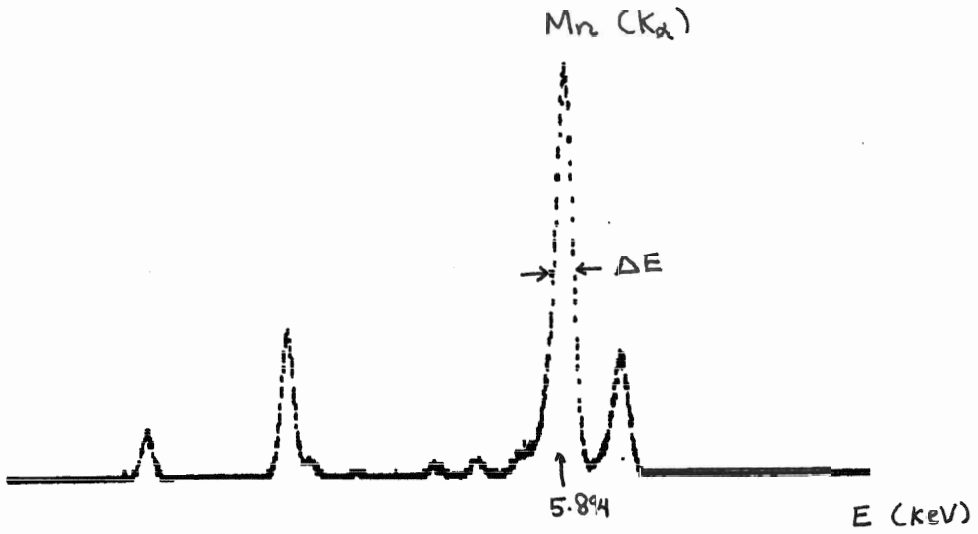


Figure (3-6) The energy resolution $\Delta E$ of the detector obtained from the energy spectrum of Fe source.

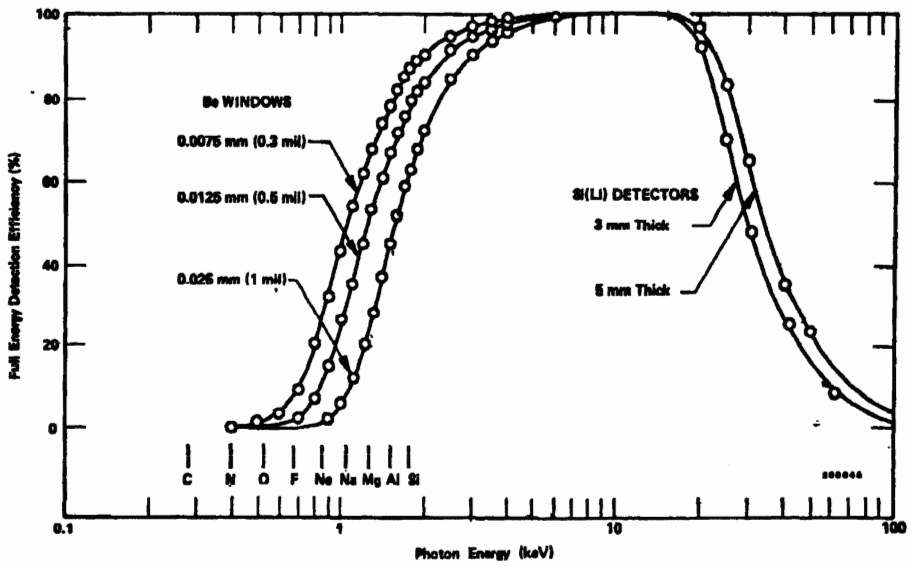


Figure(3-7) The efficiency of detection of x-rays by Si(Li) detector.

(d) Slit For Diffraction Acceptance Angle:-

A lead(Pb) sheet which has a 1mm slit is positioned in front of the Be window. This slit will permit only a portion of the diffracted beam to go through the Be window. Therefore, the slit accepts only those rays diffracted in the direction within the diffraction interval ($\Delta\theta$). As result of reducing the acceptance angle to that interval, the energy interval $\Delta E$ defining the diffraction line decreases, thus reducing the width of the diffraction lines.

(2) The Multi-channel Analyzer (MCA):-

The voltage pulses produced by the detector are sent to the main amplifier for further amplification. Those amplified pulses are then received by the MCA computer which will sort them out according to their amplitudes [12]. Pulses with identical amplitudes are stored at the same memory channel. There are 1000 channels in the MCA display. Since the amplitude is proportional to the energy of the photon absorbed by the detector, photons of various energies appear in the MCA display as counts in different channels. The relation between the energy (E) and the channel number (N) is a linear one given by $E = aN+b$.

The display is energy calibrated by using two or three fluorescence lines of known energies at different channels in the spectrum. The MCA computer determines (a) and (b) thereby converting the display from channel to energy scale.

# (4) Experimental Procedures

## (4-1) Sample Preparation:-

There are different ways of preparing a sample from powder material. One method for preparing a sample is by pressing the powder into a tablet form. This method is suited for our apparatus since a tablet sample could be easily mounted and reused as target. However, preparing the sample by this method may result in a problem which affect the measured intensities of the diffraction lines. Pressing the grains which make up the powder may cause a preferred orientation of those grains [12]. When the grains have preferred orientation, the contribution to the intensities of the lines would not be accurate. This is because the diffraction from some planes occurs at the expense of other planes. Therefore, the intensity distribution of the diffraction pattern would not represent the true pattern of the material analyzed.

Another method of preparing a sample from the powder is by packing the powder into a thin walled glass tube [11,12,19]. This is inconvenient for the EDXD system for two reasons. One is the difficulty of mounting the tube. The second is the absorption of the beam coming in and out of the tube. The latter arises because the absorption in the tube is not constant as result of the continuous nature of the beam.

A mechanism for holding the Al powder was designed in such way that the preferred orientation of the grains is minimized and in such a way that the sample could be easily mounted and reused as target. This holder, which is described in the apparatus section, contains the Al powder

without pressing it and at the same time directly exposes the powder to the incident beam.

For the room temperature part, the Al powder was packed in the holder as follows:

(1) The hollow disc was placed on top of a smooth glass slide.

(2) The Al powder was packed into the 20 mm diameter hole.

(3) The powder was then mixed with a binder diluted in amyl acetate so as to hold the grains together and with the disc.

(4) After cleaning off the excess of the powder that spilled over the disc surface, the second piece of the holder was placed on top and connected to the first piece.

(5) The assembly was then turned upside down so that the glass slide became on top of the holder.

(6) The glass slide was very gently slide off the the Al powder surface in order to obtain smooth surface of the Al powder.

(7) The powder was left to dry off.

Three Al samples (Al#2, Al#3, Al#4) were prepared by mixing with different amount of the binder material to see if the diffraction pattern was affected by the binder. A fourth sample (Al#1) was prepared by mixing the powder with water to see if the powder would hold together. Mixing with water worked. The powder held together and it did not spill out when the the sample was rotated or turned up side down.

For the high temperature part, the samples were prepared by mixing the powder with water in the cavity of the solid disc. The Al powder was smoothed to coincide with the level of the disc holder surface.

## (4-2) Indexing And Identification of The Al Diffraction Lines:-

The diffraction pattern from the (Al#1) sample was used for the identification and the indexing of diffraction lines. The incident beam used to obtain the diffraction pattern was produced by the tube operated at 20 kv and 15 mA. The incident beam consisted of photons with energies in the range of 1-20 kev. The diffraction angle ($2\theta$) was set approximately to 30°. Figure (4-1) shows this diffraction pattern. Four of the lines present in the spectra are diffraction lines. The other three lines which are located at the lower energy region of the spectra were identified as the fluorescence lines of Fe (E=6.458 keV), Cu (E=8.106 keV),and Zn (E =8.721 keV). The source of the Cu and the Zn lines was determined to be a scattering of the incident beam from the edge of the collimator. As for the Fe line, the source could be the Mo tube itself.

The most intense of the four diffraction lines is positioned at E=9.512 keV. The known diffraction pattern of Al from the powder diffraction file shows that the (111)plane with (d) spacing of 2.338 $A^{\circ}$ produces the most intense line [20]. The Bragg condition for the EDXD state that the product of the energy of the line and the plane spacing is constant, i.e

$$E.d = \frac{6.2}{\sin\theta}.keV.A^{\circ} = \text{constant}$$

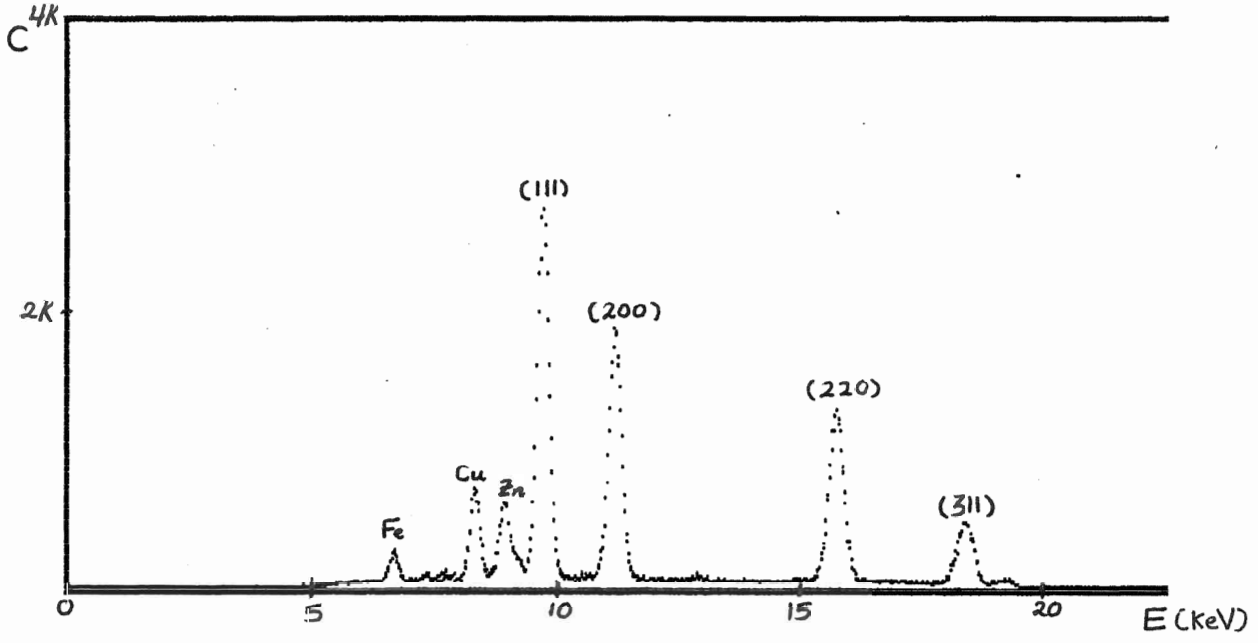


Figure (4-1) The spectra of the Al diffraction pattern obtained at $2\theta=32°$.

Making use of this relation and the fact that the the (111) line is the most intense line in the obtained spectra. Then,

$$E.d = 9.512 \times 2.338 = 22.239 \text{ keV.A}^\circ$$

The values of (d) for the other planes in the spectra are

$$d_{(hkl)} = (22.239/E_{(hkl)}).$$

**Table (4-1):-**

The indexing and the identification of the lines present in the obtained spectra and comparing their (d) value with those from the expected Al diffraction pattern [20].

| **Expected values** | | **Experimental values** | | | |
|---|---|---|---|---|---|
| (hkl) | d (A°) | E (keV) | E.d | θ | d (A°) |
| 111 | 2.338 | 9.51 ±0.01 | 22.239 | 16 | 2.338±0.003 |
| 200 | 2.024 | 10.98±0.01 | " | " | 2.025±0.002 |
| 220 | 1.431 | 15.53±0.01 | " | " | 1.432±0.001 |
| 311 | 1.221 | 18.14±0.01 | " | " | 1.226±0.001 |

The experimental values of (d) show excellent agreement with the expected values. Therefore, by comparison the diffraction lines present in the spectra were identified to be the (111), (200), (220), and (311) lines.

The diffraction angle was then increased to obtain other lines which otherwise cannot be obtained at small angles because of the energy limit of the incident beam (<20 kev). Figure (4-2) shows the diffraction pattern of (Al#1) at a diffraction angle approximately equal to 50°. In this spectrum the lines identified previously shifted to the small energy region of the spectrum and other unidentified lines now appear. Because of the large resolution of the detector, some of the closely spaced lines were not resolved. However, the energy of those overlapped lines could be identified. The (111) line identified previously was now shifted to the lower energy region (E=5.997 keV). Hence,

$$E.d = 5.997 \times 2.338 = 14.021 \ \text{keV.A°}.$$

Now using this new constant nine diffraction lines were identified and compared to the expected values as shown in table (4-2). The experimental (d) values show excellent agreement with the expected values. The lines which overlapped were identified as: the (311) line overlaps with the (222)line, and the(331) with the (420). The other diffraction lines present in the spectra were identified as: the (111), (200), (220), (400), (420).

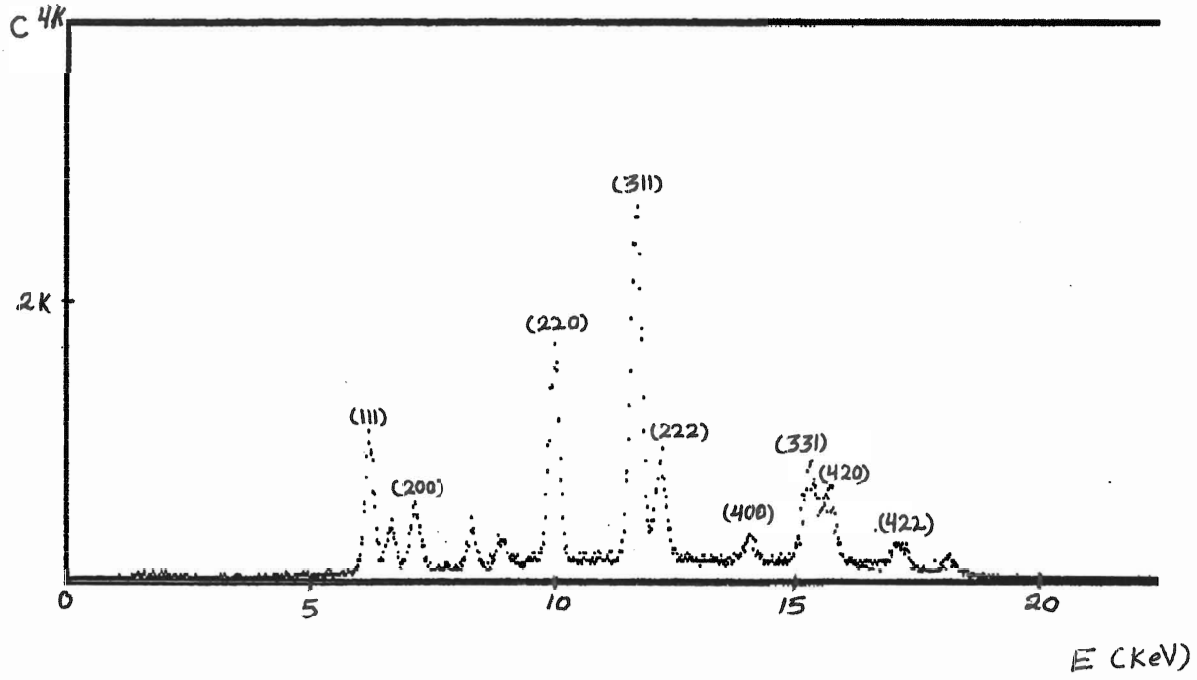


Figure (4-2) The Al diffraction pattern obtained at $2\theta = 52.4°$

**Table (4-2):-**

This table shows the identification of the lines present in the spectra which was obtained at $2\theta=52.4°$ and compared to the expected values.

| **Expected values** | | **EDXD experimental values** | | | |
|---|---|---|---|---|---|
| Line | d (A°) | E (kev) | E.d | θ | d (A°) |
| 111 | 2.338 | 6.00 ±0.01 | 14.021 | 26.2 | 2.338 ±0.004 |
| 200 | 2.024 | 6.94 ±0.01 | " | " | 2.020 ±0.003 |
| 220 | 1.431 | 9.82 ±0.01 | " | " | 1.428 ±0.002 |
| 311 | 1.221 | 11.51±0.01 | " | " | 1.218 ±0.001 |
| 222 | 1.164 | 12.02±0.01 | " | " | 1.167 ±0.001 |
| 400 | 1.0124 | 13.86±0.01 | " | " | 1.012 ±0.001 |
| 331 | 0.9289 | 15.11±0.01 | " | " | 0.9280±0.0005 |
| 420 | 0.9055 | 15.49±0.01 | " | " | 0.9054±0.0005 |
| 422 | 0.8266 | 16.96±0.01 | " | " | 0.8268±0.0005 |

## (4-3) Sample Rotation:-

The Al powder used in preparing the four samples for room temperature measurement is not very fine and contains grains of various sizes (≈3-175 μ). The integrated intensity of the diffraction line is proportional to the number and the size of the grains. Because of this large variation in the sizes of the grains, the number and the orientations of the grains exposed to the incident beam will vary from sample to another or even in the same sample from one position to another. This would result in inaccurate and unreproducible intensity measurements.

One way to reduce the effect of the variation in the grain sizes on the reproducibility and the accuracy of the measured intensity is by rotating the Al sample holder about its axis [12]. In rotating the sample the incident beam will be moving in a circular motion on the surface of the Al powder thereby exposing a larger number of grains of different sizes and orientations to it. A diffraction measurement obtained from rotated sample is equivalent to an averaging of several measurements obtained from different positions on the surface of a stationary sample.

To examine the effect of rotation on the reproducibility of the measured intensity, two sets of diffraction measurements were obtained from the four Al samples at ($2\theta \approx 30°$). One set is accumulated while the samples were not rotated and the other while they were rotated. Figure (4-3) and figure (4-4) show the overlapped spectra from the samples Al(#1-#4) with and without rotation respectively. The integrated intensities of the diffraction lines present in the spectra were measured and normalized to the (111) line. Table (4-3) contains the values of $I_R$ from the unrotated

C

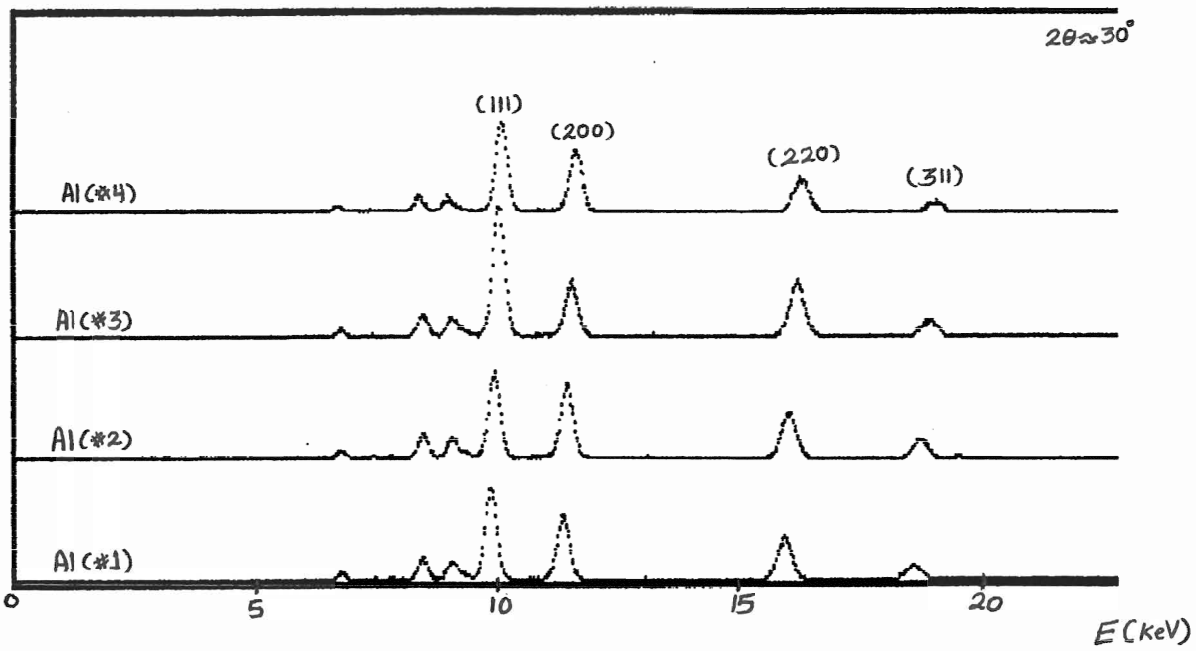


Figure(4-3) The comparison of spectra from samples Al(#1-4) obtained while they were not rotated.

C

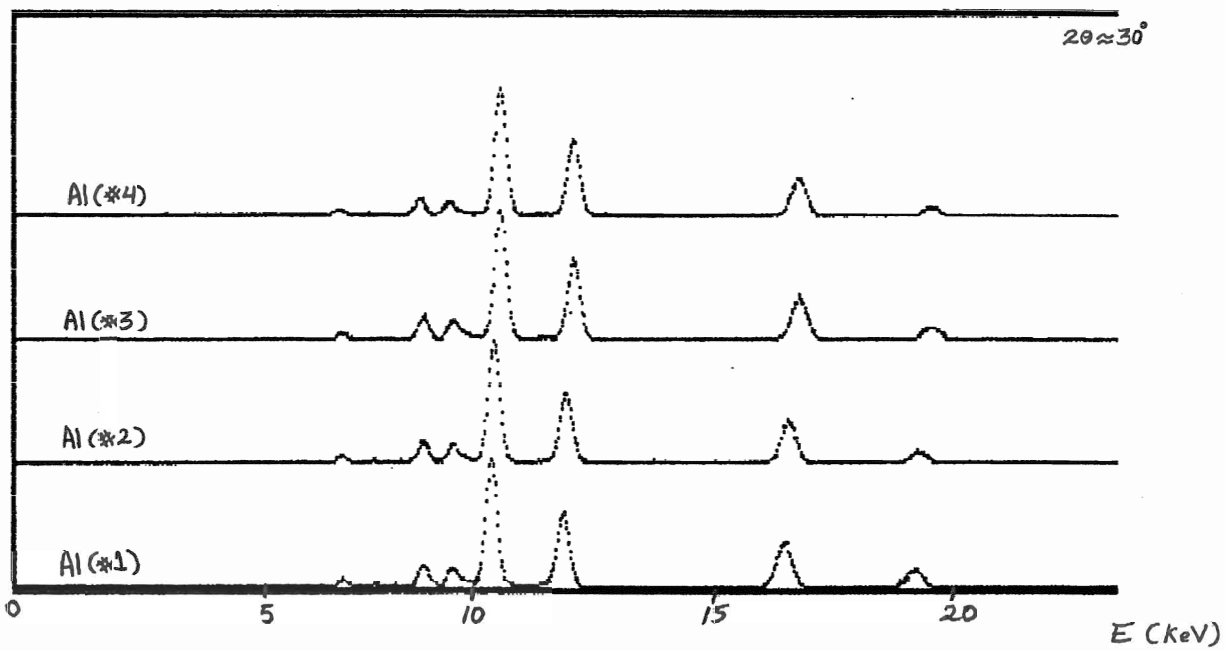


Figure (4-4) The comparison of spectra from the rotated Al(#1-4) samples.

samples. As expected the $I_R$ data in this table was inconsistent and was not reproduced from one sample to another. On the other hand, in table (4-4), which contains the values of $I_R$ from the rotated samples, the data is much more consistent. This illustration clearly demonstrates the benefit of rotating the samples. Finally, it should be noted that the diffraction pattern from the four samples did not contain interference effect from the binder material.

**Table (4-3):-**

The relative intensity measurements ($I_R$) from unrotated samples.

| Line | AL#1 | AL#2 | AL#3 | AL#4 |
|---|---|---|---|---|
| 111 | 100 | 100 | 100 | 100 |
| 200 | 74±1 | 90±1 | 40±1 | 74±1 |
| 220 | 46±1 | 69±1 | 50±1 | 48±1 |

**Table (4-4):-**

The values of $I_R$ from rotated samples

| Line | AL#1 | AL#2 | AL#3 | AL#4 |
|---|---|---|---|---|
| 111 | 100 | 100 | 100 | 100 |
| 200 | 64±1 | 62±1 | 64±1 | 62±1 |
| 220 | 46±1 | 42±1 | 42±1 | 38±1 |

## (4-4) Powder Annealing:-

Strains and damage to the Al grains, which may have resulted from the production of the powder, may affect the intensity of the diffraction [11,12]. To fix the strains and damage to the grains the Al powder was annealed. Annealing the powder causes the atoms in the damaged area to rearrange their positions thereby fixing the damage.

Two Al samples were prepared from annealed powder. One sample was prepared from powder annealed for 6 hrs. at T=550° C while the second was prepared from powder annealed at the same temperature but for a longer period of time (24 hrs.). The powder was annealed for different times to examine if that has an effect on the measured intensity. The powder was annealed in vacuumed tubes to avoid any oxidation of the Al. The two Al samples were prepared from the annealed powder by mixing with water and using the same process described previously.

## (4-5) Powder Sieving :-

The large variation of the Al grain sizes causes a problem with regard to the reproducibility of the measured intensity. One way of eliminating this problem is by rotating the powder. Another way of avoiding the problem is by eliminating the large variation of the grain sizes. Reducing the average size of the grains would increase the number of the grains which have the correct orientation to contribute to the intensity [11,12]. This would result in a more reproducible intensity measurements. Therefore, the powder was sieved through meshes of

different sizes to obtain the smallest average size of the grains(≈3-60 μ with average size of ≈30 μ ).

To illustrate this advantage several diffraction measurements on a sieved Al sample were carried out at (2θ≈30). In each measurement the beam was incident on different position on the surface of the sample which was held fixed. Table (4-5) shows the $I_R$ data normalized to the (111) line from those measurements. This data shows clearly more consistency and reproducibility compared to the $I_R$ data in table(4-3) obtained from unsieved powder.

**Table (4-5):-**

The $I_R$ from sieved sample. Three measurements were taken from different positions of the unrotated sample and one from the sample while it was rotated.

| Line | Position#1 | Position#2 | position#3 | Rotation |
|---|---|---|---|---|
| 111 | 100 | 100 | 100 | 100 |
| 200 | 62 | 56 | 56 | 61 |
| 220 | 35 | 35 | 34 | 36 |

The samples which were used in the high temperature part were all prepared from the finest powder obtained by sieving. Also, one sample from this fine powder was prepared for the room temperature part.

## (4-6) Measurement Of The Shape Of The Incident Beam:-

Since the incident X-ray beam used in the EDXD is continuous, the incident intensity ($I_{0(hkl)}$) will vary from one diffraction line to another. In order to calculate the expected $I_R$ the incident intensities, at which the lines occur, have to be known. The only way of knowing them is by measuring the shape of the continuous x-ray beam.

The measurement of the incident beam spectra was as follows: the x-ray beam was produced at voltage of (20 kv) which was the same as the voltage used for the diffraction measurements. Having identical voltages is essential since the shape of the beam spectra is related to the voltage. The beam was then incident directly into the detector. At this particular geometry the detector might be jammed because of its exposure to a very large number of photons. The number of photons incident were reduced by lowering the tube current to a very minimum level of ($\approx$ 1 mA) and by introducing Pb containing a (.036 mm) pin hole in front of the collimator to reduce the size of the (1 mm) beam. The small pin hole allowed us to look at different portions of the beam. Figure (4-5) shows the overlapping spectrum of different portions of the beam. The shape of the spectra, which were accumulated for different times, appear to be identical. Therefore, this leads to the conclusion that the beam is uniform.

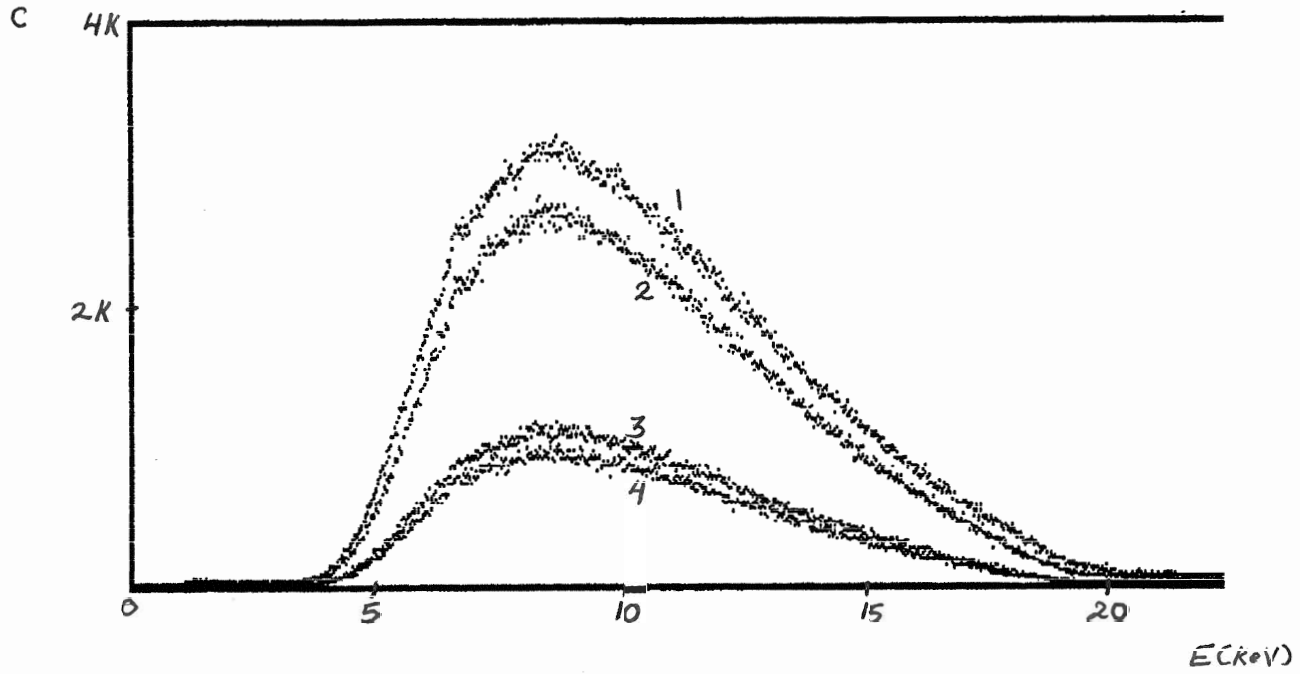


Figure (4-5) The comparison of spectra of the incident beam from different measurements

The shape of the measured spectra is the result of the product of the beam intensity ($I_0$) and the detector efficiency ($\varepsilon$). The measured intensity for a particular line ($I_{0(hkl)}$) is given by the number of counts in the region of the spectra where the line is located. Table (4-6) contains the intensities ($I_0$) of different regions of the incident beam spectra obtained from different measurements. Those intensities were normalized to the intensity of the (390-405 Ch.) region. The data shows that the lower and the middle region are the most stable. The stability decreases in the upper region because of the sensitivity of this region to voltage fluctuations.

**Table (4-6):-**

The relative intensities of different regions of the incident beam spectra.

| Meas. | $I_0\varepsilon$ (390-405) | $I_0\varepsilon$ (520-535) | $I_0\varepsilon$ (630-645) | $I_0\varepsilon$ (740-755) | $I_0\varepsilon$ (850-765) |
|---|---|---|---|---|---|
| #1 | 1.00 | 0.76 | 0.47 | 0.24 | 0.08 |
| #2 | 1.00 | 0.76 | 0.46 | 0.23 | 0.06 |
| #3 | 1.00 | 0.75 | 0.45 | 0.22 | 0.04 |
| #4 | 1.00 | 0.76 | 0.45 | 0.22 | 0.04 |

## (5) Measurement Of Relative Intensity ($I_R$) At Room Temperature

### (5-1) procedures:-

In this section the intensities of the lines in the Al diffraction pattern were measured. The measured intensities of lines were normalized to a specific line in the spectra in order to obtain the relative intensities ($I_R$). To examine the reproducibility of the ($I_R$) data, the diffraction measurements were obtained from four differently prepared samples. Those samples are;

(1) Al (#4), prepared from unsieved powder.

(2) Al (sieved), prepared from sieved powder.

(3) Al (6 hrs..), prepared from unsieved annealed powder.

(4) Al (24 hrs..), prepared from unsieved annealed powder.

The diffraction pattern consisting of the(111), (200), and(220) line was obtained at $2\theta \approx 30°$. At $2\theta \approx 50°$, the pattern consisted of nine lines (see identification section). The diffraction measurements were carried out while the samples were rotated except for the Al(sieved) sample. The compared spectra of the four samples are shown in figure (5-1) for the small angle and in figure (5-2) for the larger angle.

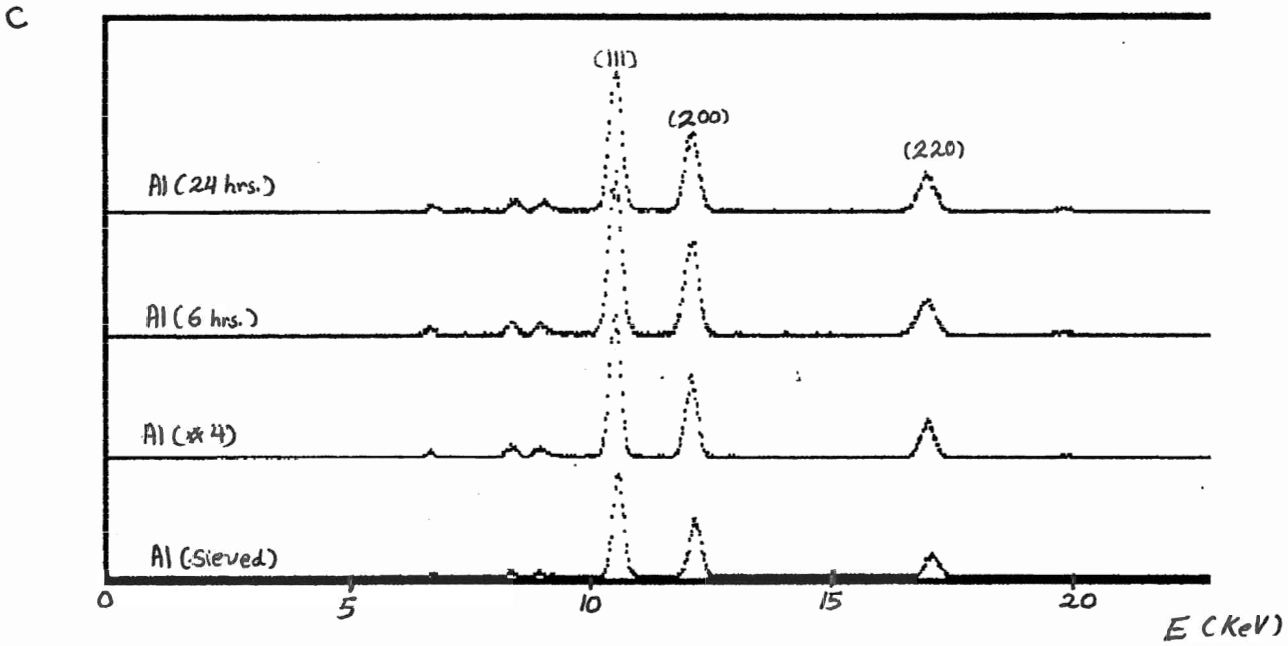


Figure (5-1) The comparison of spectra from four different Al samples at $2\theta \approx 30°$

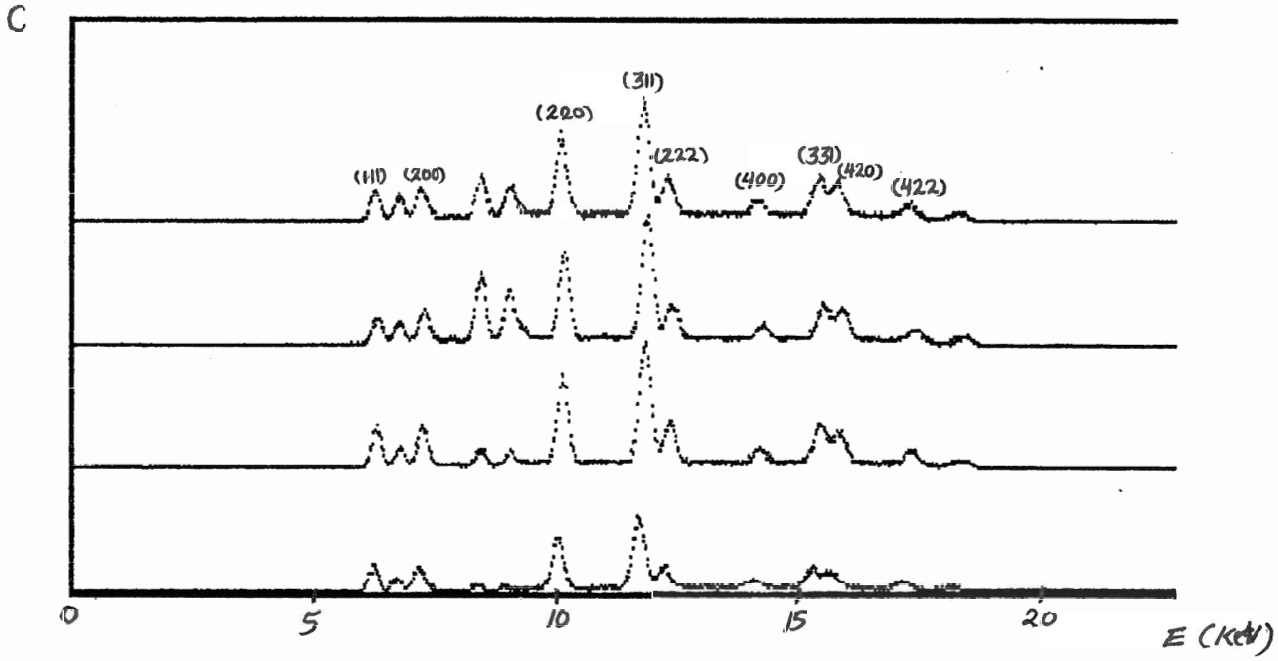


Figure (5-2) The comparison of spectra from The four Al samples at $2\theta \approx 50°$.

## (5-2)The Method Of Measuring The Intensity:-

The intensity of a line is given by the integrated intensity of the peak which is measured by the area of the peak above the back ground. This area which is measured in terms of the counts accumulated under the peak is defined by a region of interest. The region of interest is set by scanning an equal number of channels in both sides of the center of the peak. The region of interest will determine the gross counts accumulated under the peak which includes the back ground counts. Figure (5-3) shows the region of interest set for the (111) line. The net counts which measure the integrated intensity is given as

Net Counts (N.C)=Gross Counts (G.C)-Back Ground (B.G).

The back ground is determined by the counts under a straight line drawn between the first and the last channel in the region of interest. The MCA determines the (G.C), the (B.G), and the(N.C).

For the un resolved lines in the diffraction pattern obtained at $2\theta \approx 50°$, the region of interest was set to include the two overlapped lines thereby measuring the combined integrated intensity. Table (5-1) shows the integrated intensities from the four samples, and it also shows the ($I_R$) obtained by normalizing to the (111) line for the small angle and to the (220) line for the larger angle. The integrated intensities of the (111) and (200) lines in the large angle pattern could not be measured because of the interference of the Fe $K_\alpha$ line (see fig. 5-2).

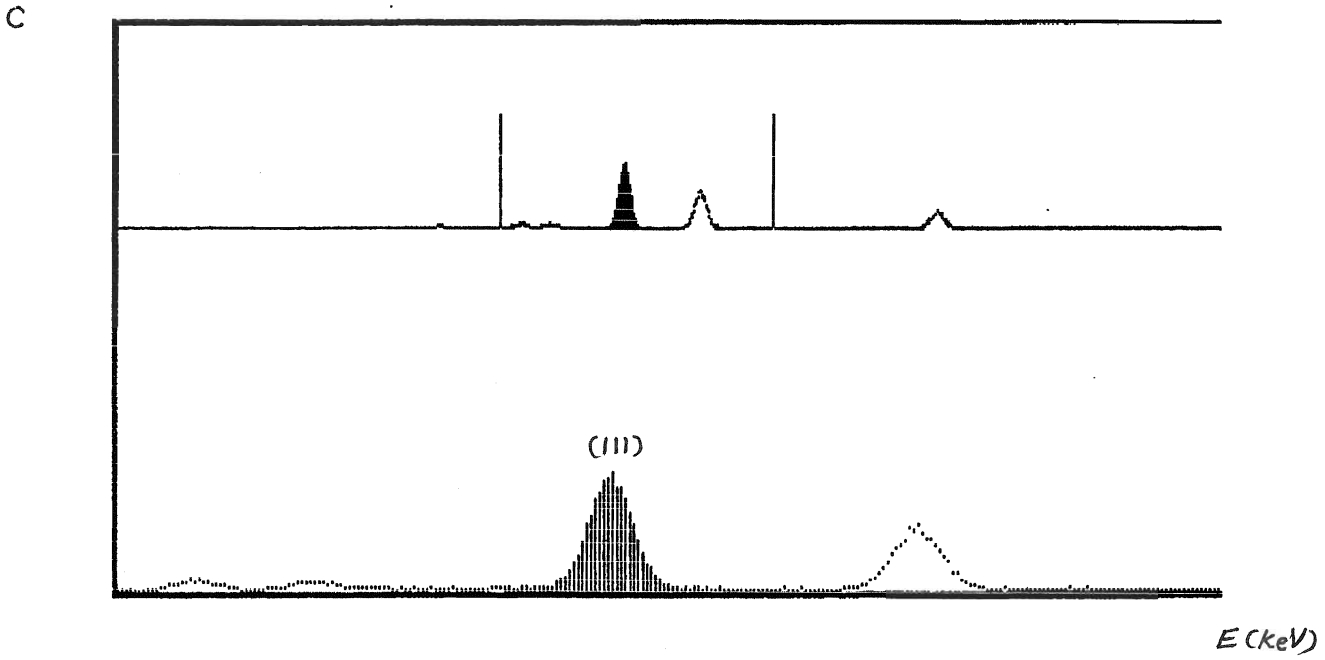


Figure (5-3) The region of interest set for the (111) line producing a gross of (15543 C) and net of (13962 C).

**Table (5-1):-**

The integrated intensities of Al powder diffraction lines obtained at two angles and from four samples. The table contains the net counts (N.C) and the relative intensity ($I_R$).

| 2θ=30 | | | | | | | | |
|---|---|---|---|---|---|---|---|---|
| Line | Al (#4) | | Al (Sieved) | | Al (6 hrs) | | Al (24 hrs) | |
| | N.C | $I_R$ | N.C | $I_R$ | N.C | $I_R$ | N.C | $I_R$ |
| 111 | 13962 | 100 | 10217 | 100 | 17840 | 100 | 16549 | 100 |
| 200 | 8482 | 61±1* | 6438 | 63±1 | 11961 | 67±1 | 10262 | 62±1 |
| 220 | 4446 | 32±1 | 3230 | 32±1 | 5627 | 32±1 | 5828 | 35±1 |
| 2θ=50 | | | | | | | | |
| 220 | 8320 | 100 | 5240 | 100 | 7905 | 100 | 7341 | 100 |
| 311+222 | 16608 | 200±4 | 10057 | 192±6 | 16861 | 213±6 | 15896 | 216±6 |
| 400 | 1496 | 18 ±1 | 988 | 19 ±2 | 1196 | 15 ±1 | 1456 | 20 ±2 |
| 331+420 | 7574 | 91 ±3 | 4615 | 88 ±4 | 7502 | 95 ±3 | 7650 | 104±3 |
| 422 | 1717 | 21 ±1 | 1159 | 22 ±1 | 1663 | 21 ±1 | 1499 | 20 ±1 |

## (5-3) Comments About The Intensity Data:-

* Note:- The error was given by the statistical precision of the integrated intensity, i.e

$$\%\sigma\ (N.C) = \frac{\sqrt{G.C+B.C}}{N.C} \times 100$$

$$I_R = \frac{(N.C)_1 \pm \%\sigma_1}{(N.C)_2 \pm \%\sigma_2}$$

Hence, $\%\sigma\ (I_R) = \%\sigma_1 + \%\sigma_2$,

$\sigma(I_R) = \%\sigma(I_R) \times I_R$

-The $I_R$ data obtained from the four samples are consistent and reproduced within a margin of ≈10% for all lines except the (400) line.

-The order of most intense to the least intense is reproduced and consistent through out the data.

-The intensity data contains contribution from other scattering called thermal diffuse scattering (TDS). This scattering results in a very broad maxima coinciding with the Bragg maxima. The correction of TDS would reduce the values of the $I_R$.

## (5-4) Calculations, results, & Discussion:-

### (1) Calculation of the TDS correction to the integrated intensity:-

The procedure used to measure the integrated intensity is by subtracting a straight line back ground as shown as shown in figure(5-4). Therefore, the intensity of the peak includes a contribution from TDS. To enhance the accuracy of the measured intensity, the correction to eliminate the TDS contribution has to be made [21,22]

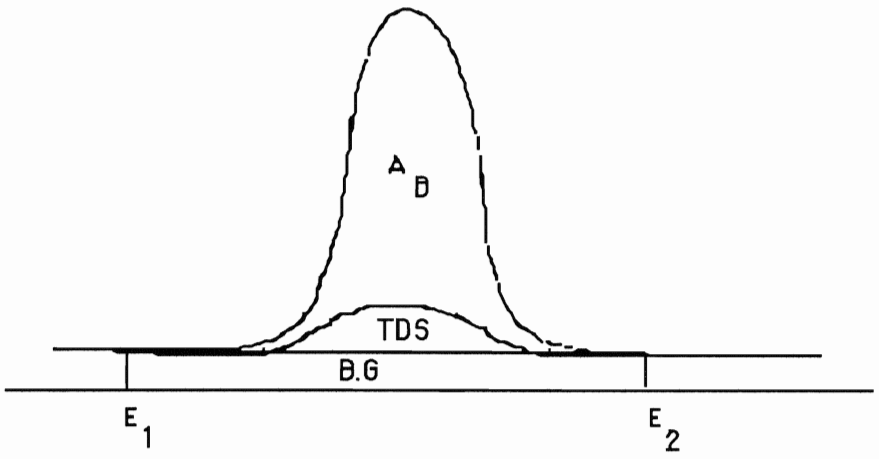


Figure (5-4) The Bragg peak and the TDS above the straight line back ground

The correction factor for a particular peak is given as [21]

$$\sigma = \frac{A_{TDS}}{A_{Bragg}}, \qquad \text{Where A is the area.}$$

$$\sigma = (\frac{\pi}{3})^2 M_D \, a \, \Delta \frac{\cos\theta}{\lambda}$$

Where a is the lattice parameter, $M_D = B(T).(\frac{\sin\theta}{\lambda})^2$ is the DWF, and $\Delta$ is the total length of the region of the interest for the Bragg peak in $2\theta$ expressed in radians.

The corrected intensity is given as

$$I_{corrected} = \frac{I_{measured}}{1+\sigma}$$

In the EDXD, $\Delta$ is measured in terms of of E. Therefore, $\Delta$ in terms of E is converted in terms of $2\theta$ through the Bragg equation, i.e

$$\theta = \sin^{-1}(\frac{6.2}{d.E})$$

The calculation for the TDS correction factor is carried out for the Al lines in table (5-2).

**Table (5-2):-**

The calculation of the TDS correction factor $\sigma$ for the lines obtained from sample Al (#4) at ($2\theta \approx 30, 50$).

| Line | $\lambda$(A°) | $\theta$ | $M_D$ | $E_1$ (kev) | $E_2$ (kev) | $2\theta_1$ | $2\theta_2$ | $\Delta$ (rad.) | $1+\sigma$ |
|---|---|---|---|---|---|---|---|---|---|
| 111 | 1.221 | 15.1 | 0.045 | 9.618 | 10.713 | 32.0 | 28.6 | 0.059 | 1.009 |
| 200 | 1.058 | " | 0.060 | 11.174 | 12.269 | 31.8 | 28.9 | 0.051 | 1.012 |
| 220 | 0.750 | " | 0.120 | 15.889 | 17.200 | 31.7 | 29.2 | 0.044 | 1.045 |
| 220 | 1.269 | 26.2 | 0.120 | 9.226 | 10.324 | 56.0 | 49.6 | 0.112 | 1.039 |
| 311 | 1.081 | " | 0.166 | 10.917 | 12.017 | 55.4 | 50.0 | o.094 | 1.057* |
| 222 | 1.036 | " | 0.181 | 11.422 | 12.522 | 55.4 | 50.1 | 0.093 | |
| 400 | 0.899 | " | 0.240 | 13.246 | 14.344 | 55 | 50.5 | 0.079 | 1.078 |
| 331 | 0.824 | " | 0.285 | 14.498 | 15.596 | 54.8 | 50.7 | 0.072 | 1.094* |
| 420 | 0.803 | " | 0.299 | 14.893 | 15.991 | 54.7 | 50.7 | 0.070 | |
| 422 | 0.735 | " | 0.358 | 16.343 | 17.441 | 54.6 | 50.9 | 0.065 | 1.117 |

* Note:- For the combined lines $\sigma_{total} = (A_{TDS1}+A_{TDS2})/(A_{B1}+A_{B2})$

Where, $A_{TDS} = A_B \times \sigma$.

$$\therefore \quad \sigma_{total} = (A_{B1} \times \sigma_1 + A_{B2} \times \sigma_2)/(A_{B1}+A_{B2})$$

$$= \sigma_1(A_{B1}/[A_{B1}+A_{B2}]) + \sigma_2(A_{B2}/[A_{B1}+A_{B2}])$$

$$\approx (\sigma_1+\sigma_2)/2.$$

(2) Calculation of the intensity:-

The intensities of the Al lines were calculated in this section for the purpose of comparison with the experimental values. The calculated intensity was obtained using the EDXD modified $I_R$ equation given as $I_R = (I_0\mathcal{E})\,|F|^2\,P\,\exp[-2M]\,(1/\mu)\,(1/E^2)$.

(1) $I_0\mathcal{E}$ is the incident intensity at which the line occurs in the incident beam spectrum. It is measured for different lines by setting equal regions of interest at the positions where the lines are located. The number of counts under those regions give the incident intensities. Since the calculated intensities are normalized to the (111), and the (220) lines, the incident intensities are normalized to the incident intensities of those two lines.

(2) E is the energy at which the line center is located. The values of E used in the calculation correspond to the lines obtained from the sample Al(#4) at $2\theta \approx 30°, 50°$.

(3) P is the multiplicity factor for a cubic crystal and it is obtained for each line from table (2-1)

(4) |F| is structure factor for the (fcc) cell of Al. It is given as [1]

$|F| = 4f$ when h,k, and l are unmixed

$=0$ " " " " mixed

f (the atomic scattering factor) is measured for each line from the graph in figure (2-3).

(5) exp[-2M] (the temperature factor) is obtained by using the value of B(T) at room temperature corresponding to the HHS potential in table (2-2) the values of B(T) corresponding to this potential are the closest to the values of B(T) obtained by other experimental method.

(6) $\mu$ ( the linear absorption coefficient) is obtained from the graph of $(\mu/\rho)$ vs.$\lambda$ shown in figure (2-5). The density of Al ($\rho$) cancels out when $I_R$ is calculated.

The calculation procedure for the intensities of the Al lines which were obtained at two diffraction angles were carried out in table (5-3). The theoretical equivalence to the measured intensity of the overlapped lines was obtained by calculating the intensity of each line separately then adding them together

**.Table (5-3):-**

The values of the factors affecting the calculated intensity for each diffraction line and the calculated intensities for the nine Al lines.

| Line | E (kev) | θ | f | $\|F\|^2$ | P | $(\mu/\rho)$ $(cm^2/g)$ | $e^{-2M}$ | $I_0\varepsilon$ | I |
|---|---|---|---|---|---|---|---|---|---|
| 111 | 10.157 | 15.1 | 8.8 | 1239 | 8 | 26.00 | 0.913 | 1.00 | 519 |
| 200 | 11.717 | " | 8.4 | 1129 | 6 | 17.50 | 0.887 | 0.80 | 307 |
| 220 | 16.525 | " | 7.1 | 807 | 12 | 6.72 | 0.787 | 0.23 | 147 |
| 220 | 9.771 | 26.3 | 7.1 | 807 | 12 | 29.10 | 0.787 | 1.00 | 422 |
| 311 | 11.467 | " | 6.4 | 655 | 24 | 18.60 | 0.717 | 0.805 | 570 |
| 222 | 11.972 | " | 5.9 | 557 | 8 | 16.50 | 0.697 | 0.73 | 148 |
| 400 | 13.809 | " | 5.5 | 484 | 6 | 11.00 | 0.619 | 0.49 | 65 |
| 331 | 15.047 | " | 5.1 | 416 | 24 | 8.68 | 0.566 | 0.36 | 159 |
| 420 | 15.442 | " | 5.0 | 400 | 24 | 8.16 | 0.549 | 0.34 | 142 |
| 422 | 16.868 | " | 4.4 | 310 | 24 | 6.32 | 0.487 | 0.19 | 59 |

Results & discussion:-

The relative intensity results obtained experimentally from the four Al samples are compared to their corresponding calculated results in table (5-4). The experimental and the calculated results show fairly good consistency and agreement in the order from the most intense line to the least intense lines. Both show that the (111) line is the most intense in the obtained Al diffraction pattern and they also show that the (400) and the (422) lines are the least intense.

To examine the effect of annealing on the $I_R$ results, the experimental results from the annealed and the unannealed were compared separately. The experimental results from the unannealed samples Al(#4) and Al(sieved) show excellent agreement and consistency with each other within the statistical errors. This shows that rotating the sample produced equivalent effect on the measured intensity as that produced by sieving the powder. The experimental results from the two annealed samples show very slight effect from annealing on the $I_R$ results. The results from the annealed samples are a little scattered and are less consistent with each other, for example, the $I_R$ value from the Al(24 hrs.) and the Al(6 hrs.) are (19 and 14) respectively for the (400) line. This difference of 25% is much larger than the statistical error. Also, annealing produced a slight increase in the values of $I_R$ for most of the lines compared to the values of $I_R$ from the unannealed samples, for example, there is 10% increase in the value of $I_R$ for the combined lines (331+420).

**Table (5-4):-**

The experimental values of $I_R$ from the four Al samples corrected for the TDS and compared to their corresponding calculated values.

| Line | Al#4 | Al(sieved) | Al(6 hrs) | Al(24 hrs) | Calculated |
|---|---|---|---|---|---|
| 111 | 100 | 100 | 100 | 100 | 100 |
| 200 | 61±1 | 63±2 | 67±1 | 62±1 | 59 |
| 220 | 31±1 | 31±1 | 31±1 | 34±1 | 28 |
| 220 | 100 | 100 | 100 | 100 | 100 |
| 311+222 | 197±4 | 189±6 | 209±6 | 212±6 | 170 |
| 400 | 17±1 | 18±1 | 14±1 | 19±2 | 15 |
| 331+420 | 86±3 | 84±3 | 90±3 | 99±3 | 71 |
| 422 | 19.5±1 | 20±1 | 19.5±1 | 19±1 | 14 |

In addition to the consistency of the experimental result from the unannealed samples, those results are closer to the calculated results compared to the results from the annealed samples. In table (5-5) the average of the experimental results for the unannealed samples and the average from the annealed samples are compared to the calculated results. When comparing the experimental results with the calculated, the closest agreement occurs for the (200) line with 5% difference for the unannealed results and 10% difference for the annealed results. This difference between the experimental and the calculated results increases for the other lines to reach ≈40% for the (400) line. The large discrepancy between the experimental and the calculated values for the weak lines may be due to an error caused by the precision of setting the region of interest and the subtracting of the back ground. Also, the intensities of the lines located in the upper region of the spectra may be affected by the sensitivity of this region to voltage fluctuations.

It should be pointed out the accuracy of the calculated values of $I_R$ are affected by the precision and the reliability of the values of several factors ($I_0\varepsilon$, f, $\mu/\rho$, exp[-2M]) involved in the intensity expression. Those factors have very large variation from the most intense line to the least intense line, for example, $I_0\varepsilon$ varies from (1 to 0.19). Therefore, the uncertainty of the calculated $I_R$ values should be taken into account when those values are compared with the experimental results. Table (5-6) contains the average of the experimental results compared to the to the calculated results.

**Table (5-5):-**

The average of $I_R$ from the unannealed samples and the average of $I_R$ from the annealed samples compared to the calculated $I_R$.

| Line | Unannealed<$I_R$> | Annealed<$I_R$> | Calculated $I_R$ |
|---|---|---|---|
| 111 | 100 | 100 | 100 |
| 200 | 62±2 | 65±1 | 59 |
| 220 | 31±1 | 33±1 | 28 |
| 220 | 100 | 100 | 100 |
| 311+222 | 193±5 | 210±6 | 170 |
| 400 | 18±1 | 17±2 | 15 |
| 331+420 | 85±3 | 95±3 | 71 |
| 422 | 20±1 | 19±1 | 14 |

**Table (5-6):-**

The average values of $I_R$ from the four Al samples compared to the calculated values of $I_R$.

| LINE | $I_R$ (Experimental) | $I_R$ (calculated) |
|---|---|---|
| 111 | 100 | 100 |
| 200 | 63±2 | 59 |
| 220 | 32±1 | 28 |
| 220 | 100 | 100 |
| 311+222 | 202±10 | 170 |
| 400 | 17±2 | 15 |
| 331+420 | 90±6 | 71 |
| 422 | 19.5±1 | 14 |

## (6) The Effect Of Temperature On The Intensity Of Diffraction

### (6-1) Procedures:-

In this part of the research the Al diffraction pattern was obtained at different temperatures in order to measure the effect of the change of the Al temperature on the intensity of the diffraction lines. The diffraction pattern was first measured at room temperature (R.T). This R.T measurement was used as a reference for the change that occured in the pattern as result of temperature change. The diffraction pattern was then measured at higher temperatures up to (550°C). Increasing the temperature up to 550°C achieves noticeable effect on the intensity without the risk of melting the powder ($M_p$= 650°C).

The samples used in the temperature measurements were prepared from the finest sieved powder. There was no need for rotating the sample because of two reasons. The use of sieved powder was one of the reasons (see sieving section). The second reason is that the variation of intensity with temperature is obtained by comparing the intensities of the same line at different temperatures. Therefore, regardless of the nature of the Al powder, the change that occurs in the intensity of each line is due only to the change in the temperature factor ($e^{-2M}$) with all the other factors affecting the intensity being constant.

To measure the effect of temperature on the intensities of the nine Al lines previously identified, the temperature-diffraction measurements were obtained at $2\theta \approx 30°$ and 50°. The data obtained at the

smaller angle were accumulated for half hour, whereas the larger angle data were accumulated for 2.5 hrs. because of the low counting rate.

Accurate account of the temperature is very important for this experiment. Two independent measurements of the temperature were obtained(see the high temperature apparatus section). The Mo tube was operated at 20 kv, 15 mA and the vacuum cell was at minimum pressure of 15-20 μ. The diffraction measurements were obtained from the samples Al (#5), Al (#6), and Al (#7) at the temperatures R.T, ≈250°C, ≈350°C, ≈450°C, and ≈550°C. The temperatures from different measurements varied within few degrees from those above temperatures. For samples Al (#5) and Al (#6), the measurements were carried out at the larger angle whereas for the sample Al (#7) the measurements were at the smaller angle.

Two sets of measurements were obtained for each sample. The first set included the measurements at the previously mentioned temperatures. The second set was a repeat of the first set after the samples were cooled down. Figure (6-1) shows the overlapped spectrum from the sample Al (#5) at R.T, 350, and 550° C. The intensity data from the three samples are shown in tables (6-1) to (6-4). The data is expressed as the ratio $R_T$ ($=I_{R.T}/I_T$) where $I_{R.T}$, $I_T$ represent the integrated intensity at room temperature R.T and temperature T respectively.

C

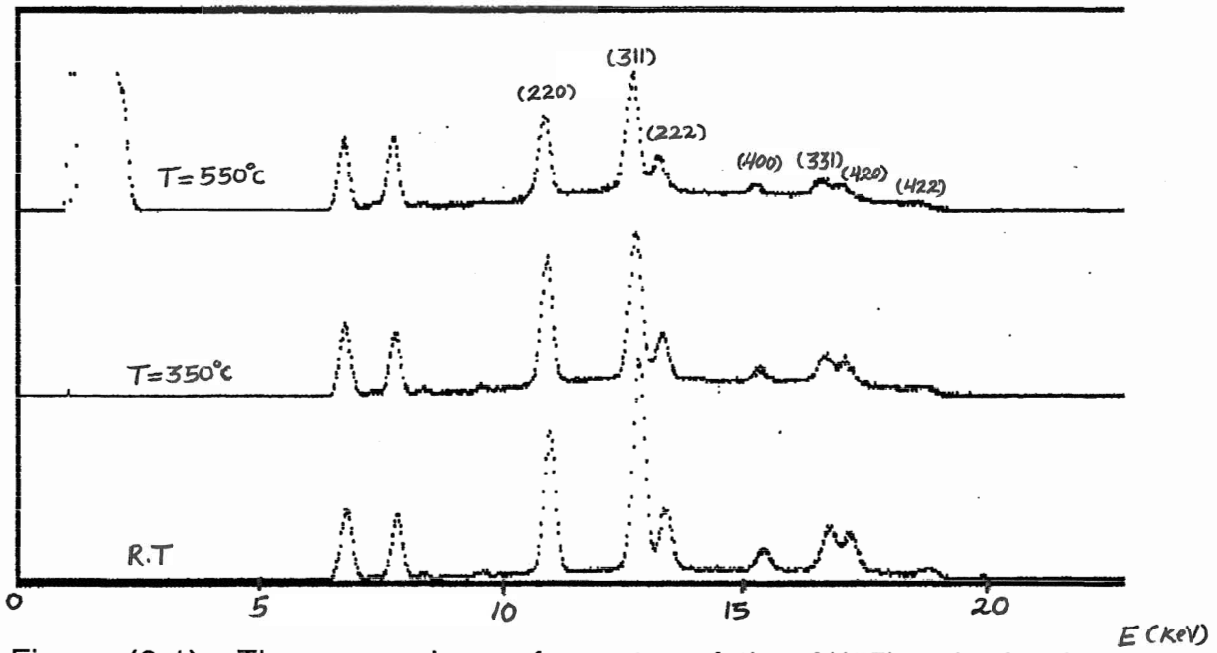


Figure (6-1) The comparison of spectra of the Al(#5) obtained at $2\theta \approx 50°$ for different temperatures

**Table (6-1):-**

Different measurements of the intensities at R.T relative to the intensities at T=250°C . The table also include those measurements after the TDS correction.

| Line | Al(#5) meas.1 | | Al(#5) meas.2 | | Al(#6) meas.1 | | Al(#6) meas.2 | |
|---|---|---|---|---|---|---|---|---|
| 2θ≈50 | $R_T$ | $R_T$-TDS | $R_T$ | $R_T$-TDS | $R_T$ | $R_T$-TDS | $R_T$ | $R_T$-TDS |
| 220 | 1.06 | 1.10±.02 | 1.19 | 1.24±.02 | 1.13 | 1.17±.02 | 0.98 | 1.02±.02 |
| 311+222 | 1.24 | 1.30±.01 | 1.11 | 1.17±.01 | 1.35 | 1.42±.01 | 1.21 | 1.27±.01. |
| 400 | 1.30 | 1.39±.10 | 1.19 | 1.27±.10 | 1.67 | 1.78±.15 | 1.56 | 1.66±.14 |
| 331+420 | 1.37 | 1.48±.03 | 1.18 | 1.27±.03 | 1.20 | 1.29±.02 | 1.33 | 1.43±.03 |
| 422 | 1.40 | 1.51±.15 | 1.39 | 1.50±.18 | 1.37 | 1.48±.20 | 1.45 | 1.57±.19 |

| Line | Al(#7) meas.1 | | Al(#7) meas.2 | |
|---|---|---|---|---|
| 2θ≈30 | $R_T$ | $R_T$-TDS | $R_T$ | $R_T$-TDS |
| 111 | 1.04 | 1.05±.02 | 0.97 | 0.98±.01 |
| 200 | 1.16 | 1.17±.02 | 1.06 | 1.07±.02 |
| 220 | 1.10 | 1.14±.02 | 1.17 | 1.22±.04 |

**Table(6-2):-**

The data of the intensities at R.T relative to T=350°C.

| Line | Al(#5) meas.1 | | Al(#5) meas.2 | | Al(#6) meas.1 | | Al(#6) meas.2 | |
|---|---|---|---|---|---|---|---|---|
| 2θ≈50 | $R_T$ | $R_T$-TDS | $R_T$ | $R_T$-TDS | $R_T$ | $R_T$-TDS | $R_T$ | $R_T$-TDS |
| 220 | 1.13 | 1.18±.02 | 1.29 | 1.35±.03 | 1.17 | 1.23±.02 | 1.09 | 1.14±.02 |
| 311+222 | 1.39 | 1.49±.01 | 1.30 | 1.40±.01 | 1.45 | 1.56±.01 | 1.44 | 1.55±.01 |
| 400 | 1.70 | 1.86±.16 | 1.48 | 1.62±.14 | 2.06 | 2.25±.22 | 2.05 | 2.24±.23 |
| 331+420 | 1.62 | 1.81±.04 | 1.56 | 1.74±.05 | 1.53 | 1.71±.05 | 1.51 | 1.68.0±5 |
| 422 | 1.95 | 2.20±.25 | 1.65 | 1.86±.22 | 1.76 | 1.98±.26 | 2.39 | 2.69±.44 |

| Line | Al(#7) meas.1 | | Al(#7) meas.2 | |
|---|---|---|---|---|
| 2θ≈30 | $R_T$ | $R_T$-TDS | $R_T$ | $R_T$-TDS |
| 111 | 1.08 | 1.09±.02 | 0.95 | 0.96±.01 |
| 200 | 1.27 | 1.30±.03 | 1.07 | 1.09±.02 |
| 220 | 1.20 | 1.26±.04 | 1.07 | 1.12±.04 |

**Table (6-3):-**

The data of the intensities at R.T relative to T= 450°C.

| Line | Al(#5) meas.1 | | Al(#5) meas.2 | | Al(#6) meas.1 | | Al(#6) meas.2 | |
|---|---|---|---|---|---|---|---|---|
| 2θ≈50 | $R_T$ | $R_T$-TDS | $R_T$ | $R_T$-TDS | $R_T$ | $R_T$-TDS | $R_T$ | $R_T$-TDS |
| 220 | 1.43 | 1.53±.03 | 1.40 | 1.49±.03 | 1.25 | 1.33±.03 | 1.27 | 1.36±.03 |
| 311+222 | 1.53 | 1.68±.02 | 1.38 | 1.52±.01 | 1.49 | 1.64±.02 | 1.49 | 1.64±.02 |
| 400 | 1.87 | 2.10±.19 | 1.54 | 1.73±.15 | 1.79 | 2.01±.20 | 2.12 | 2.38±.25 |
| 331+420 | 1.87 | 2.16±.06 | 1.76 | 2.03±.05 | 1.51 | 2.03±.05 | 1.78 | 2.05±.05 |
| 422 | 2.34 | 2.74±.34 | 2.90 | 3.40±.62 | 1.51 | 1.77±.27 | 3.05 | 3.57±.79 |

| Line | Al(#7) meas.1 | | Al(#7) meas.2 | |
|---|---|---|---|---|
| 2θ≈30 | $R_T$ | $R_T$-TDS | $R_T$ | $R_T$-TDS |
| 111 | 1.11 | 1.13±.02 | 1.01 | 1.03±.02 |
| 200 | 1.33 | 1.36±.03 | 1.20 | 1.23±.02 |
| 220 | 1.28 | 1.37±.05 | 1.45 | 1.55±.06 |

**Table (6-4):-**

The data of the intensities at R.T relative to T = 550° C.

| Line | Al(#5) meas.1 | | Al(#5) meas.2 | | Al(#6) meas.1 | | Al(#6) meas.2 | |
|---|---|---|---|---|---|---|---|---|
| 2θ≈50 | $R_T$ | $R_T$-TDS | $R_T$ | $R_T$-TDS | $R_T$ | $R_T$-TDS | $R_T$ | $R_T$-TDS |
| 220 | 1.69 | 1.84±.03 | 1.61 | 1.75±.03 | 1.52 | 1.65±.02 | 1.42 | 1.54±.03 |
| 311+222 | 1.68 | 1.88±.02 | 1.52 | 1.70±.02 | 1.83 | 2.05±.02 | 1.57 | 1.76±.03 |
| 400 | 2.22 | 2.55±.30 | 2.23 | 2.56±.29 | 3.08 | 3.54±.56 | 2.05 | 2.36±.25 |
| 331+420 | 2.53 | 3.02±.08 | 2.13 | 2.54±.06 | 1.90 | 2.26±.06 | 1.99 | 2.37±.06 |
| 422 | 5.76 | 7.01±1.7 | 5.20 | 6.32±1.9 | 6.51 | 7.92±.29 | 3.03 | 3.68±.79 |

| Line | Al(#7) meas.1 | | Al(#7) meas.2 | |
|---|---|---|---|---|
| 2θ≈30 | $R_T$ | $R_T$-TDS | $R_T$ | $R_T$-TDS |
| 111 | 1.14 | 1.16±.02 | 1.06 | 1.08±.02 |
| 200 | 1.44 | 1.48±.03 | 1.27 | 1.31±.03 |
| 220 | 1.47 | 1.60±.06 | 1.54 | 1.67±.06 |

## (6-2) Comments About The $R_T$ Data As Function Of Temperature:-

- Looking Through the $R_T$ data from tables(6-1) to (6-4), one can easily notice the expected behavior of the effect of temperature increase on the intensities of the lines. For example, $R_T$ for the (400) line increased from ≈1.52 in table (6-1), (T=250°C), to ≈2.75 in table (6-4), (T=550°C). $R_T$, which is given as $(\frac{I(R.T)}{I(T)})$, increased due to the decrease of I(T).

- Also the $R_T$ data in each table follows in general the expected effect of temperature on different lines. This effect increases the value of $R_T$ with the decreasing (d) value of the planes. For example, in table (6-4) $R_T$ increased from ≈1.1 for the (111) line to ≈6.2 for the (422). The only discrepancy in the $R_T$ values with regard to this effect occurs in the values of the (400) and the (331+420) lines. In the average, the values of $R_T$ for the(311+420) line is lower than the $R_T$ for the (400) line or, equivalently, the $R_T$ for the (400) line is higher then for (311+420) line. This inconsistency occur systematically from table (6-1) to (6-4).

- Even though the general behavior of the temperature effect on $R_T$ is consistent throughout the tables (6-1 to 4), still there is inconsistency in the reproducibility of the $R_T$ from different measurements. For example $R_T$ for the (311+222) in table (6-1) varies between 1.17 to 1.42 which is much larger than the statistical error.

- The (111) and (200), the most intense lines in the Al pattern, experience the least effect due to the increase in temperature.

- The (220) line is the only line for which the intensity was measured at both $2\theta \approx 30^\circ$ and $50^\circ$

- For the overlapped lines (311+220) and (331+420) the effect of temperature which is significant for both was measured from the combined intensities of the unresolved line.

- The (400) and (422) lines are the least intense of the lines. They both have large margin of statistical error, especially, at high temperatures when the (400) became very weak and the (420) became almost defused in the back ground.

## (6-3) Calculation, Results, & discussion:-

### (1) The effect of the instability of the incident beam intensity on $R_T$ values:-

Since the values of $R_T$ were obtained by comparing the data from independent measurements, a concern arises of how a possible change in the incident beam intensity affect the values of $R_T$. Figure (6-2) gives a comparison of two Al patterns measured for the same time, and shows that the concern over the instability of the incident beam is legitimate. The intensities of the characteristic lines of Cu, Fe, and Zn in the two compared spectrum clearly changed. This change could only be the result of change in the intensity of the incident beam. An increase in the incident intensity for a measurement at a particular temperature relative to that at R.T would result in a lower $R_T$ than expected and vice versa. However, a possible change in the incident intensity does not completely account for the

C

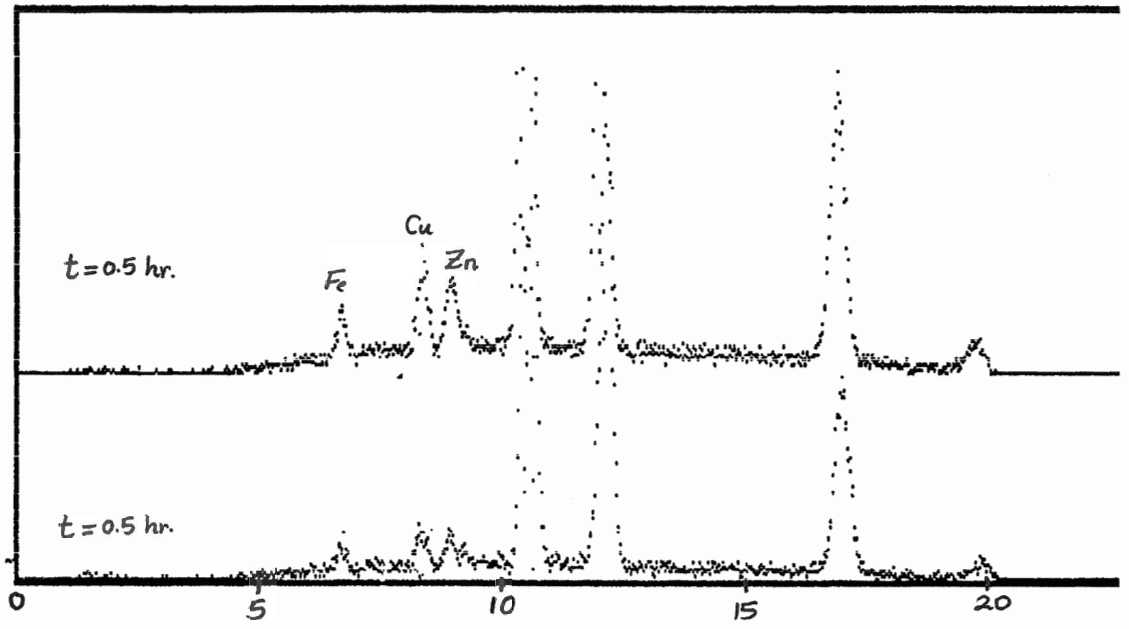


Figure (6-2) Two spectra measured for the same time showing a change in the intensities of the characteristic lines.

inconsistency and the variations of $R_T$ from different measurements. If a change in the incident beam intensity occurs,it is expected that the effect of this change is reflected on all the lines present. By looking at the data it turns out this is not the case. For example, in table (6-1) for sample Al(#6) the values of $R_T$ from the first measurement to the second measurement decreased for three lines (220, 311+222, 400) and increased for two lines (331+420 and 422). Therefore, there must be another reason beside the incident intensity variations which accounts for the inconsistency in the data. One possibility is the residual variation in the sizes of the grains (≈3-30 μ). Since the powder was not pressed, movement of the grains as result of thermal expansion may occur thereby exposing the incident beam to different number and sizes of grains.

2- Determination of the change in the DWTF B(T):-

One way of analyzing the temperature effect data is to carry it out in a way that the variations in the incident intensity is not an effective factor. This was done by taking the (ln) of the values of $R_T$, i.e

$$R_T=\frac{I_0(R.T)\exp[-2M(R.T)]}{I_0(T)\exp[-2M(T)]}, \quad \text{where } M=B(T)\,(\sin\theta/\lambda)^2$$

$$\ln(R_T)= 2[\,B(T) - B(R.T)]\,(\sin\theta/\lambda)^2+\ln[(I_0)_R].$$

This is a linear relation with the slope equal to $2(\Delta B)$ and the intercept is equal to $\ln[(I_0)_R]$. Our interest is in the slope which gives the change in the DWTF. Changes in the incident beam intensity affect only the intercept. Taking the average of $\ln(R_T)$ of the different measurements is equivalent to

**Table (6-5):-**

The effect of temperature increase on each diffraction line. $\langle \ln R_T \rangle$ is the average of the values from different measurements. $R_T = (I_{(R.T)}/I_T)$.

| Line | $(\sin\theta/\lambda)^2$ | $\langle \ln R_{250} \rangle$ | $\langle \ln R_{350} \rangle$ | $\langle \ln R_{450} \rangle$ | $\langle \ln R_{550} \rangle$ |
|---|---|---|---|---|---|
| 111 | 0.046 | 0.03±0.02 | 0.05±0.02 | 0.08±0.02 | 0.12±0.02 |
| 200 | 0.061 | 0.12±0.02 | 0.18±0.03 | 0.26±0.02 | 0.33±0.02 |
| 220 | 0.122 | 0.16±0.02 | 0.23±0.03 | 0.37±0.03 | 0.51±0.02 |
| 311+222 | 0.176 | 0.25±0.01 | 0.41±0.01 | 0.48±0.01 | 0.61±0.02 |
| 400 | 0.243 | 0.42±0.12 | 0.68±0.11 | 0.72±0.10 | 1.00±0.19 |
| 331+420 | 0.296 | 0.31±0.03 | 0.55±0.03 | 0.68±0.03 | 0.93±0.03 |
| 422 | 0.363 | 0.42±.0.12 | 0.77±0.13 | 1.17±0.16 | 1.79±0.29 |

the averaging of the intercepts of the different measurements plotted separately. Table (6-5) contains the average of the $\ln(R_T)$ of the different runs for each line and it also contains the effect of temperature increase on this average. The result of temperature effect in the table follows the expected behavior in two directions. In one direction the increase of temperature for each line leads to the increase of the quantity of $<\ln R_T>$. In the other direction the effect of temperature on different line shows the increase of of $<\ln R_T>$ with the increase of the value of $(\sin\theta/\lambda)^2$. The only discrepancy is with regard to the order of this effect on the (400) and (331+420) lines. The effect on the (331+420) is systematically less than that on the (400). It is not understood what caused this inconsistency.

3- Results & Discussion:-

The experimental results in table (6-5) were plotted as $<\ln R_T>$ vs. $(\sin\theta/\lambda)^2$.in figures (6-3) to (6-6). Each experimental graph was compared to two theoretical graphs corresponding to the Morse and HHS potentials. Those two potentials produce the minimum and the maximum of the B(T) values in table (3-2). A least square fit is drawn for the experimental points. Most of the experimental points lie in between the two theoretical fits representing the two potentials. Only the points representing the (331+420) always fall short of following the the expected behavior. The statistical error on the experimental points for (400) and (420) line is very large especially at the higher temperature but within their error they always follow the expected behavior. At the lower temperatures the experimental points are closer to the Morse fit except at the highest temperature when the effect is most significant, the points are closer to the

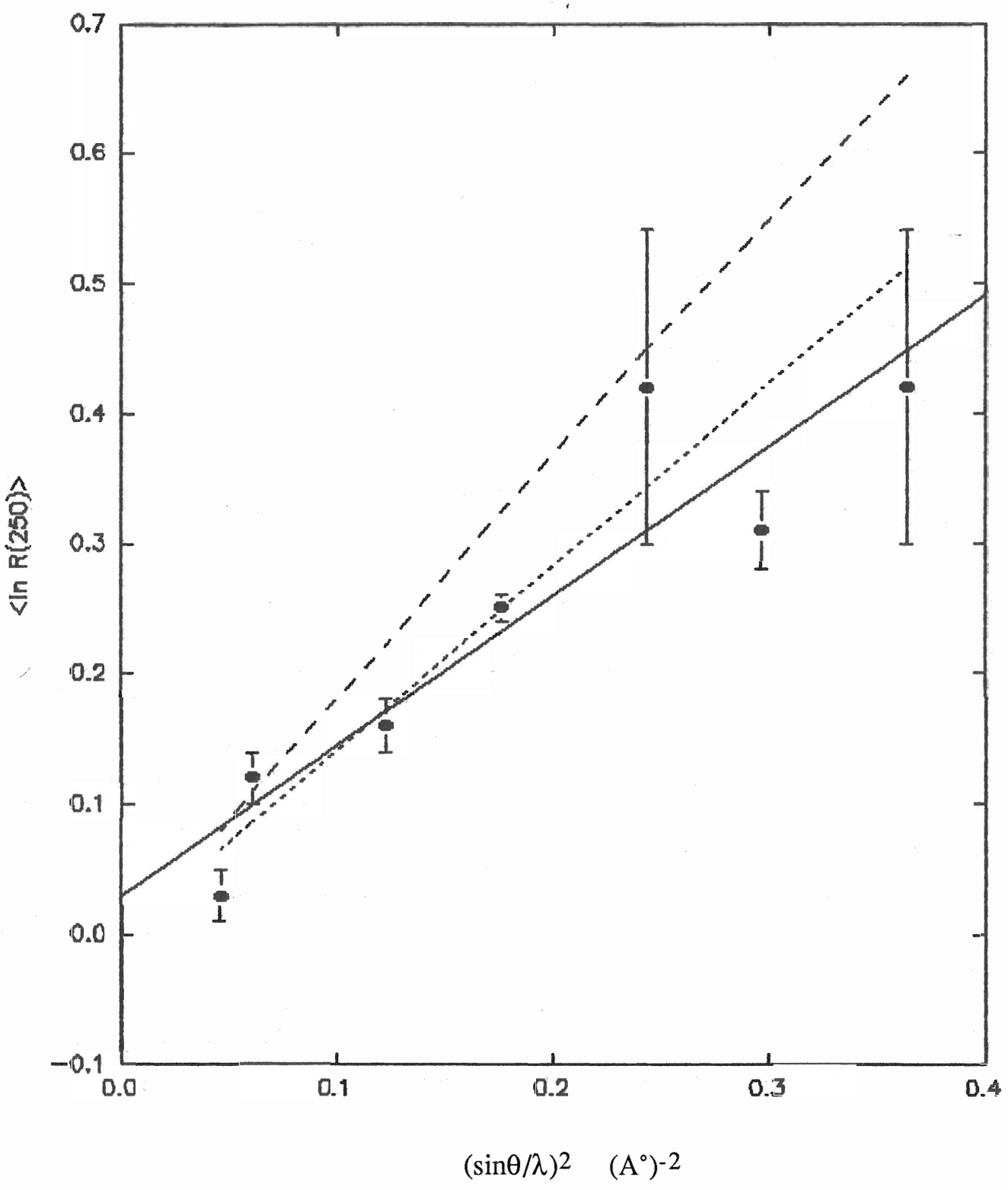


Figure (6-3) The temperature effect at 250°C on the intensity. Dots indicate experimental results. The theoretical results: Morse (short dash curve), HHS (long dash curve)

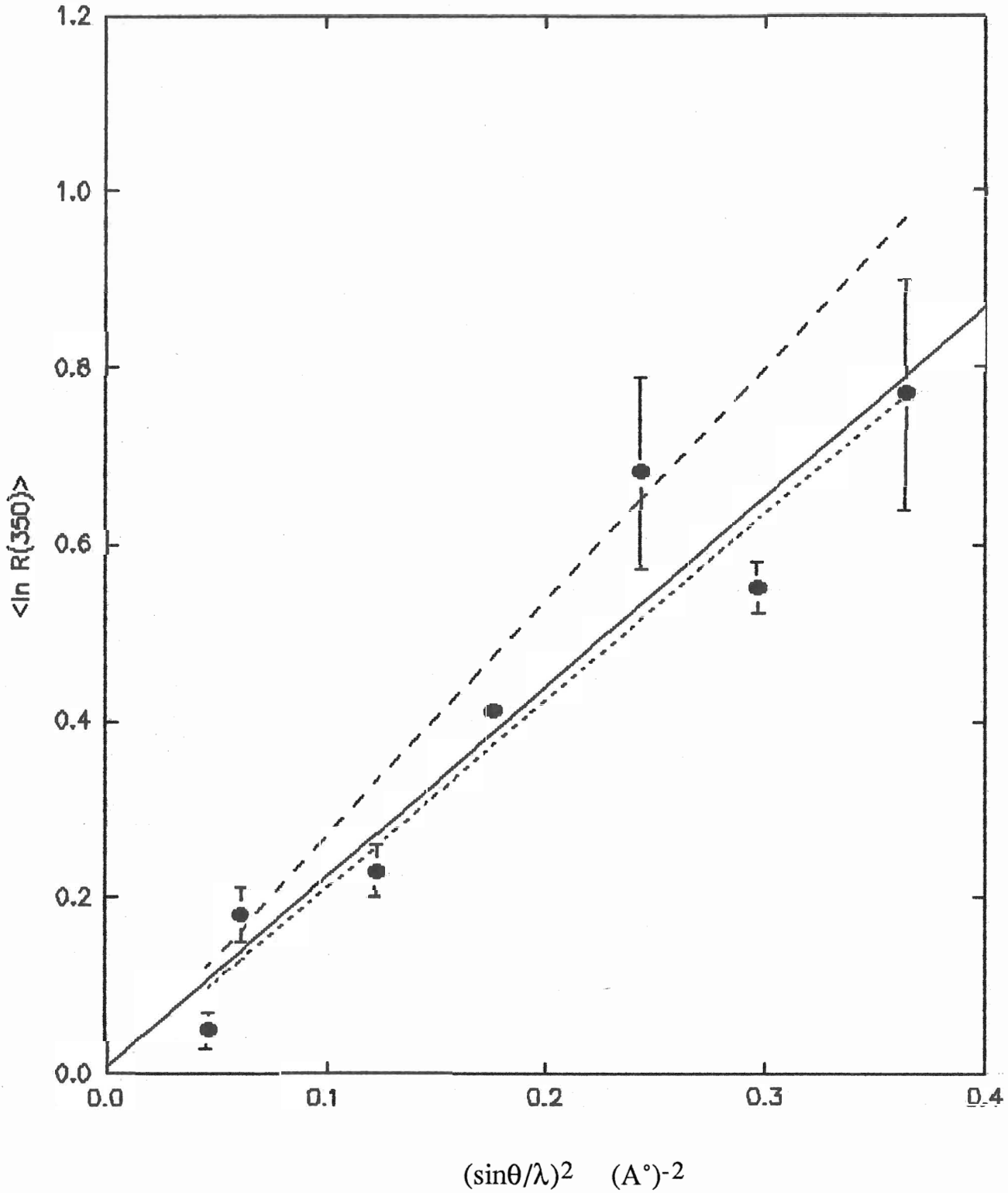


Figure (6-4) The temperature effect at 350°C on the intensity. Dots indicate experimental results. The theoretical results: Morse (short dash curve), HHS (long dash curve)

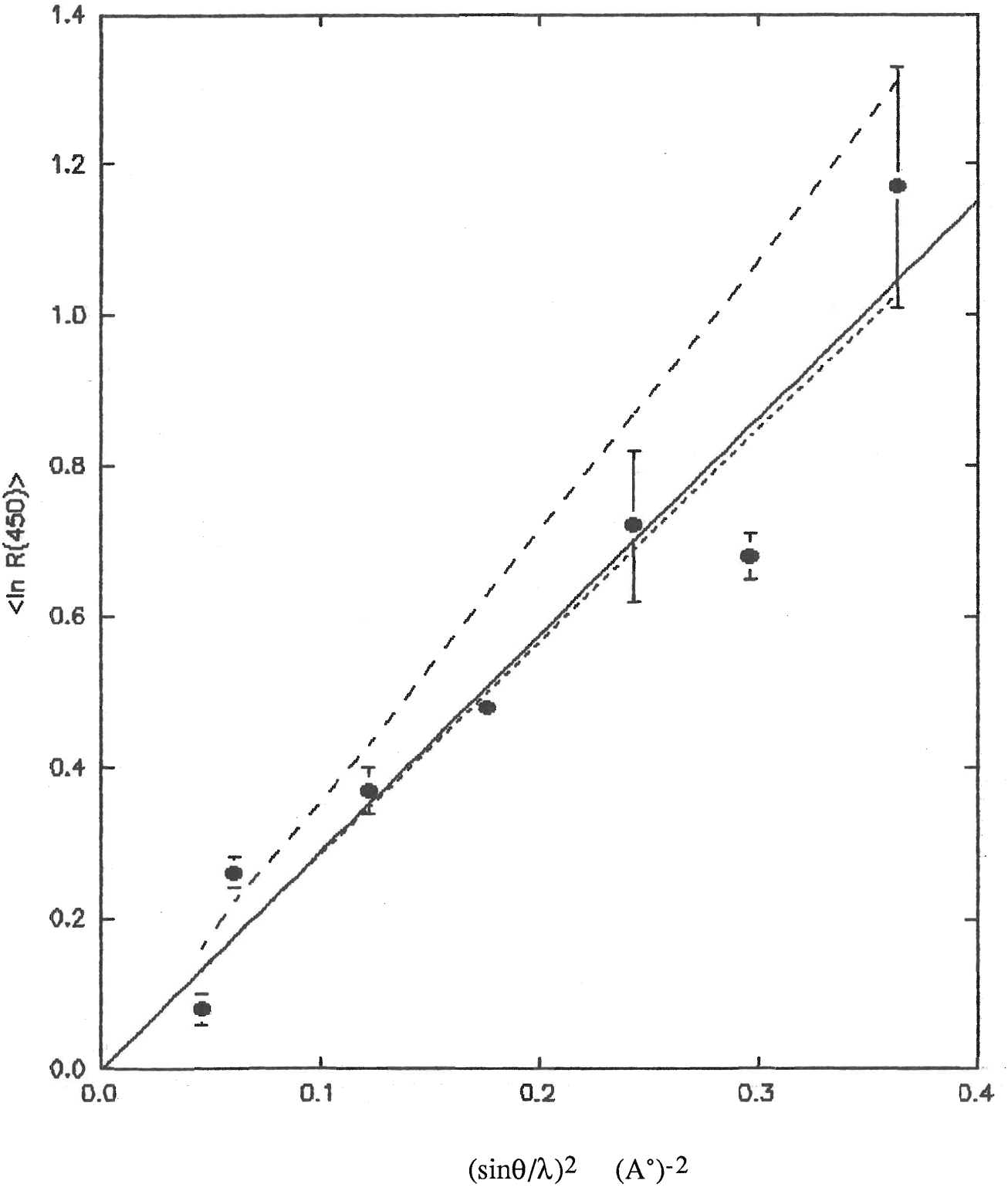


Figure (6-5) The temperature effect at 450°C on the intensity. Dots indicate experimental results. The theoretical results: Morse (short dash curve), HHS (long dash curve)

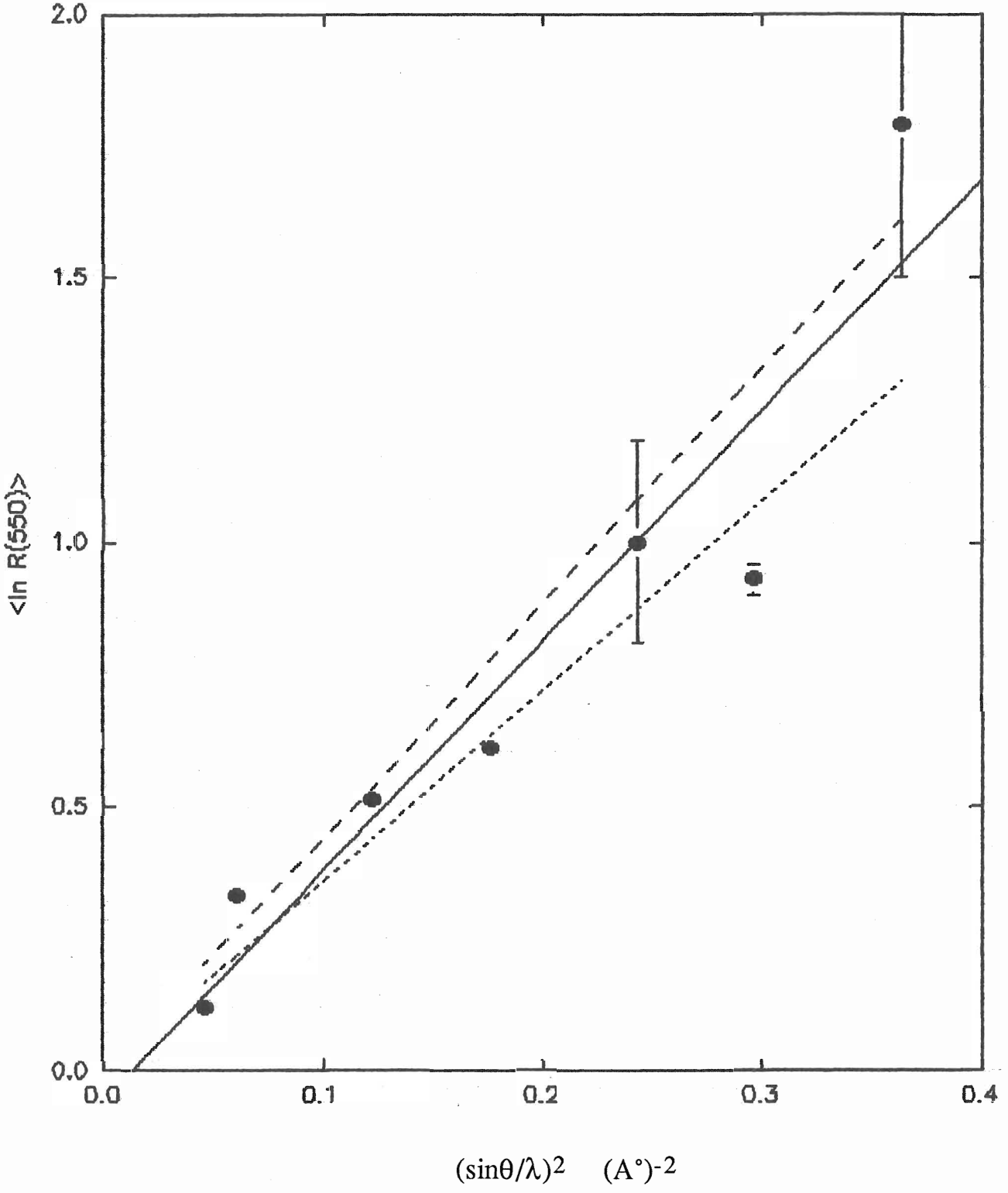


Figure (6-6) The temperature effect at 550°C on the intensity. Dots indicate experimental results. The theoretical results: Morse (short dash curve), HHS (long dash curve)

HHS fit.

The experimental values in the difference of the DWTF $\Delta B(T)$ relative to the R.T value were obtained from the slope of the best fit, i.e $\Delta B$= slope/2. The experimental result of $\Delta B(T)$ were then compared to the theoretical values corresponding to the HHS and Morse potentials as shown in table (6-6). Within the error the experimental values agree more with the values corresponding to the Morse potential except at the highest temperature (550°C) the experimental value is more comparable to the theoretical value corresponding to the HHS. The large error on the points of the two weak lines affect the the accuracy of the slope and hence the accuracy of the values of the $\Delta B(T)$, especially, at the higher temperatures when those errors are very large. Therefore, due to this uncertainty, it cannot be stated definitely whether the experimental values are better comparable to the Morse or the HHS values. However, the effect of temperature on the intensity is very clear and the experimental values definitely fall in between the two extreme potentials.

The temperature increase resulted in the increase of the values of $\Delta B(T)$ from 0.6±0.1 at 250°C to 2.2±0.4 at 550°C. Since B(T) is proportional to $\langle u^2 \rangle$, the increase of the in $\Delta B(T)$ is due to the increase of $\langle u^2 \rangle$. This agrees with the theory which predict the amplitude of the thermal vibration of the atoms $\langle u^2 \rangle$increases with the increase of temperature.

**Table (6-6):-**

The final experimental results of the difference in the DWTF $\Delta B(T)$ relative to R.T. Those results are compared to the their corresponding theoretical values.

| (R.T)/T °C | Experimental | | Theoretical $\Delta B(T)$ $(A°)^2$ | |
|---|---|---|---|---|
| | slope | $\Delta B(T)$ $(A°)^2$ | Morse | HHS |
| R.T/250 | 1.2±0.2 | 0.6±0.1 | 0.7 | 0.9 |
| R.T/350 | 2.2±0.3 | 1.10±0.15 | 1.05 | 1.35 |
| R.T/450 | 2.9±0.2 | 1.45±0.20 | 1.4 | 1.8 |
| R.T/550 | 4.4±0.7 | 2.2±0.35 | 1.8 | 2.25 |

## (7) Conclusion

Even though the consistency of some of the experimental data obtained from different samples or independent measurements was not completely achieved, overall the experimental results were fairly comparable to the theoretical results. The experimental result obtained from the Al powder at room temperature as well as at high temperature lead to the conclusion that the EDXD technique proved its capability to undertake diffraction analysis. The technique showed it has the potential to be used for reliable analysis of material structure at Brock.

For this technique the key to achieving more accurate and successful diffraction analysis of material structure is in obtaining control over the the incident beam intensity. Further studies of how to control the consistency of the incident beam intensity ($I_0$) from one measurement to another should be the basis of future diffraction analysis by this technique. Other areas, in which the accuracy of the data by this technique could be improved, deals with the nature of the sample and the time of the data accumulation. Accumulation of the diffraction data for longer period of time will enhance the accuracy of the measured intensity, especially for weak diffraction lines. As for the sample, the randomness of the powder is very essential for obtaining consistent and accurate intensity measurements. The randomness of the orientation of the grains making up the powder is maximized by the use of very fine powder with minimum variation of the grain sizes and the maximum number of grains.

**References:-**

(1) B. C. Giessen. and G. E. Gordon. Science. Vol. 159. pp.973-975, 1968.

(2) T. Fukamachi, s. Hosoya, and O. Terasaki. Journal of Applied Crystallography. Vol. 6. pp. 117-122, 1973.

(3) L. Gerward, S. Mqrup, and H. Topsqe. Journal of Applied Physics. Vol.47, 3. pp. 822-824, 1975.

(4) T. Nakajima, T. Fukamachi, O. Teraski, and S. Hosoya. Journal of Applied Crystallography. Vol. 9. pp 286-90, 1976.

(5) B. Buras. and J. Staun Olsen. Journal of Applied Crystallography. Vol. 10. pp. 431-438, 1977.

(6) M. A. Baublitz,Jr., V. Arnold, and A. L. Ruoff. Review of Scientific Instrument Vol. 52, 11. pp.1616-1624, 1981.

(7) E. F. Skelton. and S.B Qadri. Review of Scientific Instrument. Vol. 54, 4. pp.403-409, 1982.

(8) G. Albanese and C Ghezzi. Physical Review B. Vol. 5. pp.1746, 1972.

(9) G. Albanese and C. Ghazzi. physical Review B. Vol 8. pp. 1315, 1973.

(10) R. M. Nicklow and R. A. Young. Phisical Review. Vol. 152, 2. pp. 591-596, 1966.

(11) B. D. Cullity. Element of X-ray Diffraction. (Don Mills, Ontario: Addison-Wesly, 1978).

(12) Harold P. Klug. and Lenord E. Alexander. X-ray Diffraction Procedures For Polycrystalline and Amorphous Materials. (New York: John Wiley & sons, 1974).

(13) C. Kittel. Introduction to Solid State Physics. (New York: John Wiley & sons, 1976).

(14) R. W. James. The crystalline State. Vol. II: The Optical Principles of The Diffraction of X-rays. (London: George Bell, 1965).

(15) H. Lipson and H. Steeple. Interpretation of X-ray Powder Diffraction Patterns (London: Macmillian, 1970).

(16) J. W. Mayer and E. Rimini. Ion Beam Handbook For Material Analysis. (New York: Academic press inc. , 1977).

(17) R. C. Shukla and H. Hubschle. Solid State Communication, Vol. 72. 11, pp. 1135-1140, 1989.

(18) EG&G Instruments and Systems. Radiation Detection Measurement Analysis. (Oak Ridge, Tn. : EG&G Ortec).

(19) H. S. Peiser, H. P. Rooksby and A. J. Wilson. X-ray Diffraction by Polycrystalline Materials. (London: Chapman & Hall, 1960).

(20) Inorganic Index to The Powder Diffraction File. (Swarthmore, Penn. : Joint committee on powder diffraction standards, 1972).

(21) D. R. Chipman and Arthur Paskin. Journal of Applied Physics. Vol. 30, 12. pp.1992-1997, 1959.

(22) D. R. Chipman and Arthur Paskin. Journal of Applied Physics. Vol.30,12. pp. 1998-2001, 1959.